

5-1-2015

Trace Element Variations in a Stalagmite from Southwest Mexico: Implications for Paleoclimate

Chad Michael Crotty

University of Nevada, Las Vegas, crotty@unlv.nevada.edu

Follow this and additional works at: <https://digitalscholarship.unlv.edu/thesesdissertations>



Part of the [Climate Commons](#), and the [Geology Commons](#)

Repository Citation

Crotty, Chad Michael, "Trace Element Variations in a Stalagmite from Southwest Mexico: Implications for Paleoclimate" (2015). *UNLV Theses, Dissertations, Professional Papers, and Capstones*. 2344.
<https://digitalscholarship.unlv.edu/thesesdissertations/2344>

This Thesis is protected by copyright and/or related rights. It has been brought to you by Digital Scholarship@UNLV with permission from the rights-holder(s). You are free to use this Thesis in any way that is permitted by the copyright and related rights legislation that applies to your use. For other uses you need to obtain permission from the rights-holder(s) directly, unless additional rights are indicated by a Creative Commons license in the record and/or on the work itself.

This Thesis has been accepted for inclusion in UNLV Theses, Dissertations, Professional Papers, and Capstones by an authorized administrator of Digital Scholarship@UNLV. For more information, please contact digitalscholarship@unlv.edu.

**TRACE ELEMENT VARIATIONS IN A STALAGMITE FROM SOUTHWEST
MEXICO: IMPLICATIONS FOR PALEOCLIMATE**

By

Chad Crotty

Bachelor of Science in Geosciences

North Dakota State University

Spring 2011

A thesis submitted in partial fulfillment
of the requirements for the

Master of Science – Geoscience

Department of Geoscience

College of Sciences

The Graduate College

University of Nevada, Las Vegas

May 2015



We recommend the thesis prepared under our supervision by

Chad Crotty

entitled

**Trace Element Variations in a Stalagmite from Southwestern Mexico:
Implications for Paleoclimate**

is approved in partial fulfillment of the requirements for the degree of

Master of Science - Geoscience

Department of Geosciences

Matthew Lachniet, Ph.D., Committee Chair

Elisabeth M. Hausrath, Ph.D., Committee Member

David K. Kreamer, Ph.D., Committee Member

Brett Riddle, Ph.D., Graduate College Representative

Kathryn Hausbeck Korgan, Ph.D., Interim Dean of the Graduate College

May 2015

Abstract

The combination of stable isotope and trace element concentrations in speleothems has been shown to be a valuable indicator for interpreting paleoclimatic conditions. Anomalous spikes in trace element concentrations have also been shown to indicate anthropogenic environmental changes to the surface, such as deforestation events. In this study, trace element concentrations (^{24}Mg , ^{25}Mg , ^{84}Sr , ^{88}Sr , ^{137}Ba , and ^{238}U) of a stalagmite (JX-6) from Juxtlahuaca Cave, in southwestern Mexico, were measured using an inductively coupled plasma mass spectrometer (ICP-MS). These trace element concentrations were compared to previously analyzed $\delta^{18}\text{O}$ and $\delta^{13}\text{C}$ values from JX-6, and to the results of previous studies comparing U concentrations in speleothems to paleoclimate. U concentrations of JX-6 were shown to correlate well with $\delta^{13}\text{C}$ and $\delta^{18}\text{O}$ values and may be a suitable proxy for soil moisture above Juxtlahuaca Cave. This study concludes that U concentrations in JX-6 may be controlled by changes in the $p\text{CO}_2$ of overlying soils in relation to plant respiration possibly linked to variations in wet season (May – November) rainfall and temperature between 240 BCE to 1800 CE. Comparison to previous studies suggests U concentrations in speleothems are controlled by local cave conditions and that U is best used as a proxy for paleoclimatic conditions with the support of additional trace element and stable isotope data. Anomalous spikes in trace element concentrations were also observed in JX-6 at ~1862, 1871, 1904, and 1933 CE. These spikes were interpreted to be caused by uranium mobilization from soils overlying the cave, possibly relating to multiple deforestation events in association with the clearing of land above Juxtlahuaca Cave for agricultural use.

Table of Contents

Approval Page.....	ii
Abstract.....	iii
Table of Contents.....	iv
List of Tables.....	vi
List of Figures.....	ix
1. Introduction.....	1
2. Background.....	3
<i>2.1 Study Area and Stalagmite JX-6.....</i>	<i>3</i>
<i>2.2 Previous [U] Studies.....</i>	<i>8</i>
<i>2.2.1 Oxidation Control Hypothesis.....</i>	<i>10</i>
<i>2.2.2 Prior Calcite Precipitation Control Hypothesis.....</i>	<i>12</i>
<i>2.2.3 Phosphorus Control Hypothesis.....</i>	<i>16</i>
<i>2.2.4 pCO₂ Control Hypothesis.....</i>	<i>19</i>
3. Methods.....	20
4. Results.....	24
<i>4.1 Stable Isotopes.....</i>	<i>24</i>
<i>4.2 Uranium.....</i>	<i>35</i>
<i>4.3 Magnesium, Strontium, and Barium.....</i>	<i>38</i>
5. Interpretations.....	41

5.1 Trace Element Anomalies.....	41
5.2 Mechanisms Controlling $\delta^{13}\text{C}$ Values and [U] in JX-6.....	43
6. Discussion.....	47
6.1 Comparison to Previous Speleothem [U] Studies.....	47
6.2 Paleoclimatic Implications.....	49
7. Conclusion.....	53
Appendix.....	55
References.....	64
Curriculum Vitae.....	67

List of Tables

Table 1	Correlation coefficients (r) for yearly interpolated $\delta^{13}\text{C}$ of JX-6 and wet season rainfall (May – November) with various running averages and yearly lags in $\delta^{13}\text{C}$ values between 1880 to 2010 CE.....	29
Table 2	Correlation coefficients (r) for yearly interpolated $\delta^{13}\text{C}$ of JX-6 and annual median temperature with various running averages and yearly lags in $\delta^{13}\text{C}$ values between 1880 to 2010 CE.....	29
Table 3	Correlation coefficients (r) for detrended yearly interpolated $\delta^{13}\text{C}$ of JX-6 and detrended wet season rainfall (May – November) with various running averages and yearly lags in $\delta^{13}\text{C}$ values between 1880 to 2010 CE.....	31
Table 4	Correlation coefficients (r) for detrended yearly interpolated $\delta^{13}\text{C}$ of JX-6 and detrended annual median temperatures with various running averages and yearly lags in $\delta^{13}\text{C}$ values between 1880 to 2010 CE.....	31
Table 5	Correlation coefficients for averaged $\delta^{13}\text{C}$ values to averaged $\delta^{18}\text{O}$ values, ^{24}Mg , $\log(^{24}\text{Mg})$, ^{238}U , and $\log(^{238}\text{U})$ from JX-6 using various running averages between 240 BCE to 2010 CE.....	33
Table 6	Correlation coefficients for averaged $\delta^{13}\text{C}$ values to averaged $\delta^{18}\text{O}$ values, ^{24}Mg , $\log(^{24}\text{Mg})$, ^{238}U , and $\log(^{238}\text{U})$ from JX-6 using various running averages between 240 BCE to 1800 CE.....	33
Table 7	Correlation coefficients for ^{238}U to averaged $\delta^{18}\text{O}$ and $\delta^{13}\text{C}$ values, ^{24}Mg , and $\log(^{24}\text{Mg})$ from JX-6 using various running averages between 240 BCE to 2010 CE.....	36

Table 8	Correlation coefficients for the $\log(^{238}\text{U})$ to averaged $\delta^{18}\text{O}$ and $\delta^{13}\text{C}$ values, ^{24}Mg , and $\log(^{24}\text{Mg})$ from JX-6 using various running averages between 240 BCE to 2010 CE.....	37
Table 9	Correlation coefficients for ^{238}U to averaged $\delta^{18}\text{O}$ and $\delta^{13}\text{C}$ values, ^{24}Mg , and $\log(^{24}\text{Mg})$ from JX-6 using various running averages between 240 BCE to 1800 CE.....	37
Table 10	Correlation coefficients for $\log(^{238}\text{U})$ to averaged $\delta^{18}\text{O}$ and $\delta^{13}\text{C}$ values, ^{24}Mg , and $\log(^{24}\text{Mg})$ from JX-6 using various running averages between 240 BCE to 1800 CE.....	37
Table A1	Significance (p) values for correlations between yearly interpolated $\delta^{13}\text{C}$ of JX-6 and wet season rainfall (May – November) with various running averages and yearly lags in $\delta^{13}\text{C}$ values between 1880 to 2010 CE (see Table 1)	56
Table A2	Significance (p) values for correlations between yearly interpolated $\delta^{13}\text{C}$ of JX-6 and median annual temperature with various running averages and yearly lags in $\delta^{13}\text{C}$ values between 1880 to 2010 CE (see Table 2).....	57
Table A3	Significance (p) values for correlations between detrended yearly interpolated $\delta^{13}\text{C}$ of JX-6 and detrended wet season rainfall (May – November) with various running averages and yearly lags in $\delta^{13}\text{C}$ values between 1880 to 2010 CE (see Table 3).....	57
Table A4	Significance (p) values for correlations between detrended yearly interpolated $\delta^{13}\text{C}$ of JX-6 and detrended annual median temperature with various running averages and yearly lags in $\delta^{13}\text{C}$ values between 1880 to 2010 CE (see Table 4).....	58

Table A5	Significance (p) values for correlations between averaged $\delta^{13}\text{C}$ to averaged $\delta^{18}\text{O}$, ^{24}Mg , $\log(^{24}\text{Mg})$, ^{238}U , and $\log(^{238}\text{U})$ from JX-6 using various running averages between 240 BCE to 2010 CE (see Table 5).....	58
Table A6	Significance (p) values for correlations between averaged $\delta^{13}\text{C}$ to averaged $\delta^{18}\text{O}$, ^{24}Mg , $\log(^{24}\text{Mg})$, ^{238}U , and $\log(^{238}\text{U})$ from JX-6 using various running averages between 240 BCE to 2010 CE (see Table 6).....	59
Table A7	Significance (p) values for correlations between ^{238}U to $\delta^{18}\text{O}$, $\delta^{13}\text{C}$, ^{24}Mg , and $\log(^{24}\text{Mg})$ from JX-6 using various running averages between 240 BCE to 2010 CE (see Table 7).....	61
Table A8	Significance (p) values for correlations between $\log(^{238}\text{U})$ to $\delta^{18}\text{O}$, $\delta^{13}\text{C}$, ^{24}Mg , and $\log(^{24}\text{Mg})$ from JX-6 using various running averages between 240 BCE to 2010 CE (see Table 8).....	61
Table A9	Significance (p) values for correlations between ^{238}U to $\delta^{18}\text{O}$, $\delta^{13}\text{C}$, ^{24}Mg , and $\log(^{24}\text{Mg})$ from JX-6 using various running averages between 240 BCE to 1800 CE (see Table 9).....	62
Table A10	Significance (p) values for correlations between $\log(^{238}\text{U})$ to $\delta^{18}\text{O}$, $\delta^{13}\text{C}$, ^{24}Mg , and $\log(^{24}\text{Mg})$ from JX-6 using various running averages between 240 BCE to 1800 CE (see Table 10).....	62

List of Figures

Figure 1	(A) Map showing location of Juxtlahuaca Cave in southwestern Mexico.....	5
Figure 2	Satellite imagery of the surface vegetation above Juxtlahuaca Cave (black) near the end of the (A) wet season (1/10/2010) and the (B) middle of the dry season (2/22/2013).....	6
Figure 3	(A) Picture of JX-6 showing the growth axis and locations of the U/Th ages (yr BP refers to years before 2010).....	7
Figure 4	Graph showing the growth rate of JX-6 between 240 BCE to 2010 CE.....	8
Figure 5	Trace element concentrations from core MD3 versus linearly interpolated ages from U-series analysis.....	11
Figure 6	Stable isotope values from core MD3 versus linearly interpolated ages calculated from U-series analysis.....	12
Figure 7	Image of light-dark bands of HS-4 (top) next to trace element concentrations and isotope values plotted against distance from the top of HS-4 (in μm).....	14
Figure 8	Cycles 7-12 from Figure 7 were partitioned into 12 equidistant points using linear interpolation and then averaged to create composite annual cycles for the trace element and stable isotope values of HS-4.....	15
Figure 9	Annual cycles, based on Ba troughs, were portioned into 12 equidistant points and then averaged to create composite annual cycles for the trace element concentrations of MND-S1.....	17

Figure 10	Maximum trace element concentrations within each cycle (minimum for Mg) plotted next to winter rainfall and annual temperature anomalies (top), and growth rate (bottom).....	18
Figure 11	Picture of the upper 120 mm of JX-6 showing locations of milled trenches along the growth axis, drawn in pencil.....	23
Figure 12	Graph showing $\delta^{18}\text{O}$ values of JX-6 between 240 BCE to 2010 CE.....	25
Figure 13	Correlation between wet season rainfall and $\delta^{18}\text{O}$ values of JX-6 (9-year lag) using 5-year running averages (top).....	26
Figure 14	$\delta^{13}\text{C}$ values of JX-6 between 240 BCE to 2010 CE in per mil VPDB.....	28
Figure 15	Annual median temperature (red), wet season rainfall totals (blue), and yearly interpolated $\delta^{13}\text{C}$ values (brown) from JX-6 between 1880 to 2010 CE.....	30
Figure 16	Detrended annual median temperature (red), detrended wet season rainfall totals (blue), and detrended yearly interpolated $\delta^{13}\text{C}$ values (brown) from JX-6 between 1880 to 2010 CE.....	32
Figure 17	Graph showing the relationships between $\delta^{18}\text{O}$ (blue), $\delta^{13}\text{C}$ (red), $\log(^{238}\text{U})$ (light purple), U (dark purple), $\log(^{24}\text{Mg})$ (light green), and Mg (green) concentrations, and the growth rate (bottom) of JX-6 between 240 BCE to 1800 CE.....	34
Figure 18	Uranium concentrations (ppm) of JX-6 between 240 BCE to 2010 CE.....	36
Figure 19	Magnesium (^{24}Mg) concentrations (ppm) of JX-6 between 240 BCE to 2010 CE.....	39
Figure 20	Graphs showing anomalous spikes in ^{84}Sr (gray), Ba (orange), U (purple), and ^{24}Mg (green) concentrations of JX-6 around 1862, 1871, 1904, and 1933 CE.....	40

Figure 21	Graph showing normalized trace element concentrations in standard deviation units between 1800 to 2010 CE.....	42
Figure 22	$\delta^{13}\text{C}$, $\delta^{18}\text{O}$, and [U] 7-point running averages plotted from JX-6 between 240 BCE to 1800 CE shown shaded in blue (above the mean) and red (below the mean).....	52
Figure A1	Histogram showing the relative frequency of $\delta^{18}\text{O}$ values of JX-6 between 240 BCE – 2010 CE (slashed bars and dashed line) and between 240 BCE – 1800 CE (light blue bars and solid line).....	55
Figure A2	Histogram showing the relative frequency of $\delta^{13}\text{C}$ values of JX-6 between 240 BCE – 2010 CE (slashed bars and dashed line) and between 240 BCE – 1800 CE (light orange bars and solid line).....	56
Figure A3	Histograms showing (A) [U] and (B) $\log(\text{U})$ of JX-6 between 240 BCE – 2010 CE (slashed bars and dashed line) and between 240 BCE – 1800 CE (purple bars and solid line).....	60
Figure A4	Histograms showing (A) $[^{24}\text{Mg}]$ and (B) $\log(^{24}\text{Mg})$ of JX-6 between 240 BCE – 2010 CE (slashed bars and dashed line) and between 240 BCE – 1800 CE (green bars and solid line).....	63

1. Introduction

Speleothems can be useful paleoclimate proxies as they record the $\delta^{18}\text{O}$, $\delta^{13}\text{C}$, and trace element (Mg, Sr, Ba, and U) variations in cave dripwaters over time at measurable concentrations. The combination of stable isotope and trace element variations recorded in a single stalagmite can be a powerful proxy for paleoclimate interpretations. For example, $\delta^{18}\text{O}$ variations in speleothems have been shown to correlate well with rainfall amount and changes in rainfall source areas (Fairchild et al., 2006; Lachniet, 2009; Cruz et al., 2005), whereas $\delta^{13}\text{C}$ values in speleothems have been shown to correlate well with long-term changes in vegetation types (C3 vs. C4) and seasonal changes in biological activity in the soils overlying caves (McDermott, 2004; Cruz et al., 2006; Hellstrom et al., 1998). The work on trace element variations in speleothems has mainly focused on using increasing Mg/Ca and Sr/Ca ratios as an indicator of prior calcite precipitation (PCP) in the epikarst during periods of decreased rainfall (Roberts et al., 1998; Fairchild et al., 2000; Cruz et al., 2007).

In contrast, few studies have looked at the variability of [U] in speleothems, and those that have, resulted in dissimilar and conflicting interpretations (Hellstrom & McCulloch, 2000; Johnson et al., 2006; Treble et al., 2003). Each one of these interpretations is based on a mechanism that either increases or decreases the leaching and transport of U from soils and groundwater to cave dripwaters, which are then incorporated into speleothem CaCO_3 . Some of the proposed mechanisms affecting speleothem [U] include changes in biological activity in the overlying soils, varying amounts of PCP in the epikarst, and changes in phosphorus concentrations in soils.

The mobility of U in groundwater can be affected by the pH, $p\text{CO}_2$, oxidation state, the amount of U complex forming species (carbonate, phosphate, fluoride, etc.) and organic material in the water. Uranium mainly occurs as U(IV) or U(VI) in groundwater, and is predominantly transported as the uranyl ion (UO_2^{2+}) under oxidizing conditions (Langmuir, 1978). Depending on the pH value, the uranyl ion may be predominately complexed with carbonates, phosphates, or fluorides. In waters with pH values above 8.5, uranyl carbonate complexes dominate (Langmuir, 1978). These

uranyl carbonate complexes have been shown to be exceptionally mobile in groundwater and soils (Zhou & Gu, 2005). Below a pH value of 8.5, uranyl fluoride and phosphate complexes dominate (Langmuir, 1978). Most uranyl minerals (e.g., carnotite, tyuyamunite, uranophane, etc.) are least soluble at pH values of ~5-8.5. However, the solubility of these minerals has been shown to increase with increasing $p\text{CO}_2$ values (Langmuir, 1978). In natural systems, increases in $p\text{CO}_2$ values are usually associated with increases in plant respiration and decomposition (Finch & Murakami, 1999). The presence of organic matter in groundwater and soils may also affect the mobility of U. Adsorption of the uranyl ion by organic matter has been shown to greatly increase between pH values of 5-8.5 (Langmuir, 1978). During this adsorption process, the more mobile U(VI) may be reduced to U(IV). The U(IV) species is prevalent under reducing conditions, and is typically immobile in soils (Zhou & Gu, 2005). All of these parameters greatly affect the mobility of U in surface waters, and therefore cave dripwaters, and may be influenced by changes in climate.

Due to site- and sample-specific controls on isotope and trace element variations, identifying the processes that affect [U] in speleothems could assist in the analysis of paleoclimatic conditions. In this study, trace element concentrations (^{24}Mg , ^{25}Mg , ^{84}Sr , ^{88}Sr , ^{137}Ba , and ^{238}U) were measured from a stalagmite (JX-6) using an inductively coupled plasma mass spectrometer (ICP-MS). These trace element concentrations were then compared to previously analyzed stable isotope measurements from JX-6 (Lachniet et al., 2012a) and to instrumental rainfall and temperature data to test hypotheses of how variations in [U] relate to changes in rainfall, vegetation, and other processes, as inferred from other speleothem proxy data. The results of this study will also be compared to other studies (Hellstrom & McCulloch, 2000; Johnson et al., 2006; Treble et al., 2003) to test previous hypotheses on the mechanisms controlling [U] in speleothems, and to test the validity of U as a proxy for paleoclimatic change. This study will also focus on the use of speleothem trace element concentrations as a possible signal for anthropogenic affects to the land surface, similar to previous studies of speleothems from other cave sites (Borsato et al., 2007).

2. Background

2.1 Study Area and Stalagmite JX-6

Stalagmite JX-6 was collected in May of 2010 from the La Sorpresa passage of Juxtlahuaca Cave, located ~250 km south of Mexico City (17.4°N, 99.2°W, 934 m a.s.l.) in a sequence of Lower Cretaceous carbonates in the Sierra Madre del Sur of southwestern Mexico (Figure 1A) (Lachniet et al., 2012a). The collection site was ~800 m from the cave entrance and below ~160 m of carbonate bedrock (Figure 1B and 1C). There is a small section of land (~0.1 km²) that has been cleared for agricultural use located above a portion of the cave (Figure 2). The soil is ~20 cm thick at the surface and C3 type tropical dry forest is the main vegetation cover (Becerra, 2005). The local climate experiences a mean annual rainfall of 1163 mm and has an annual mean temperature of 24.6 °C (Lachniet et al., 2012b). The majority of rainfall occurs during the summer months in association with the Mesoamerican sector of the North American Monsoon (Lachniet et al., 2013). The tropical dry forest exhibits great seasonal variations, transforming from lush green forest during the rainy season (May – November) to mostly brown dormant vegetation during the dry season (December – April) (Figure 2).

Lachniet et al. (2012a) previously analyzed JX-6 using U-Th disequilibrium dating and have reported high resolution $\delta^{18}\text{O}$ and $\delta^{13}\text{C}$ values for the past 2,250 years. The U-series ages are ultra-precise and exhibit a maximum error (2σ) of ± 11 years over the last 2,250 years of growth (Figure 3A), the time span used in this study. JX-6 was ~1 m tall at the time of collection and was sampled under an active drip (Figure 3B). This stalagmite is composed of white aragonite and exhibits subtle growth banding interpreted to be defined by variations in porosity (Lachniet et al., 2012a). JX-6 appears to have grown continuously over the last 2,250 years with a growth rate ranging between 0.2 to 0.6 mm/yr (Figure 4). There are no visible hiatuses occurring during this period and only minor shifts in the drip axis (Figure 3A). No relationships were observed between variations in

growth rate or shifts in drip axis to stable isotope values or trace element concentrations. Lachniet et al. (2012a) interpreted the $\delta^{18}\text{O}$ values of JX-6 to be a suitable proxy for rainfall amount in the Basin of Mexico, and compared this rainfall reconstruction to population growth and decline in key Mesoamerican cities over the last 2,250 years.

The new trace element data from this study are compared to the previously analyzed $\delta^{18}\text{O}$ and $\delta^{13}\text{C}$ values of JX-6 from Lachniet et al. (2012a). The previously analyzed stable isotope values contain sub-annual resolution over the upper 80 mm and a data point every 3-4 years for the subsequent 900 mm. The ultra-precise U-series ages combined with the high resolution stable isotope measurements make JX-6 an excellent sample to test the mechanisms controlling [U] in speleothems.

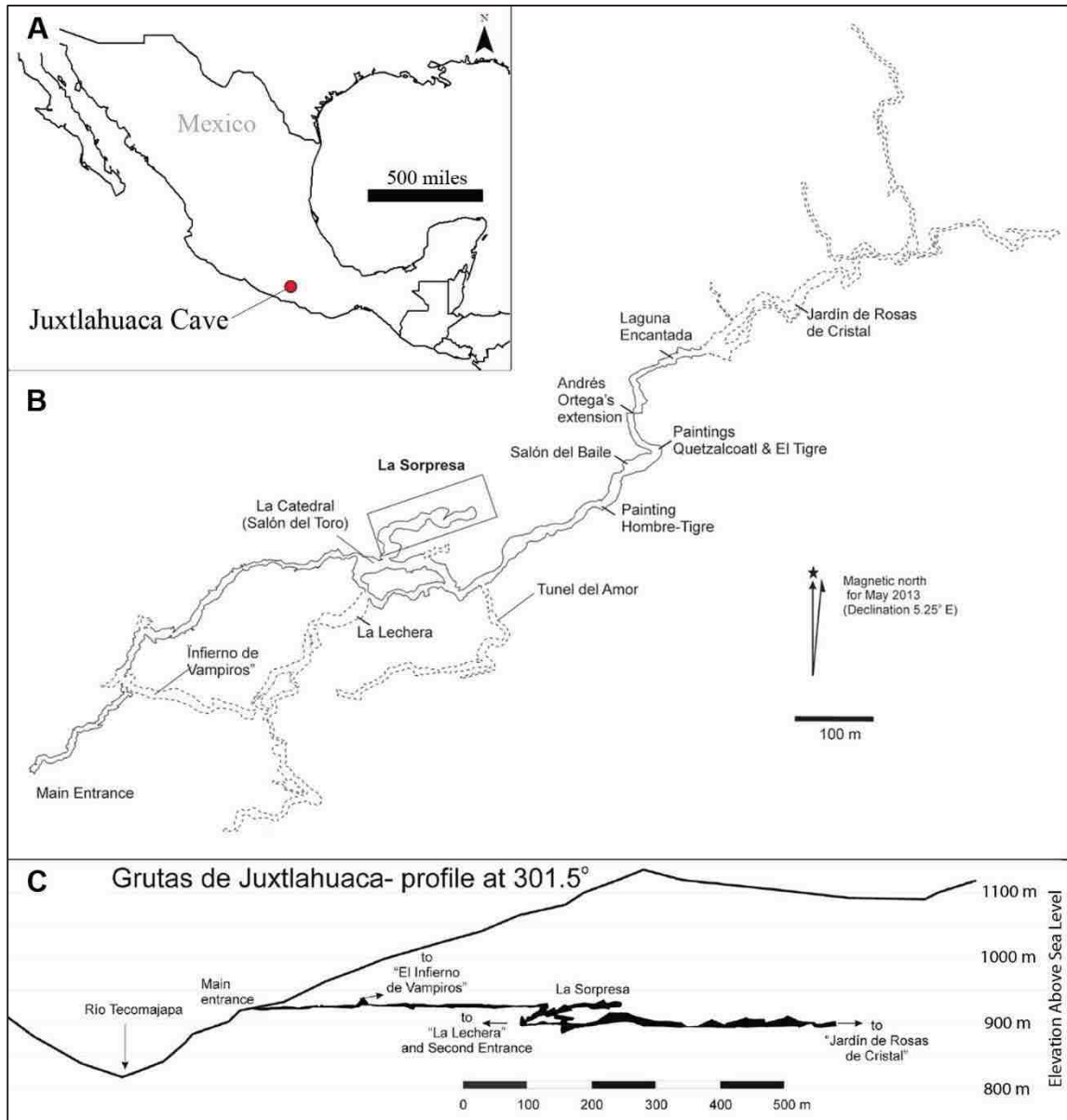


Figure 1 (A) Map showing location of Juxtlahuaca Cave in southwestern Mexico. (B) A map and (C) cross section of the cave showing the location of La Sorpresa passage relative to the main entrance. Figure modified from Rosales (2013).

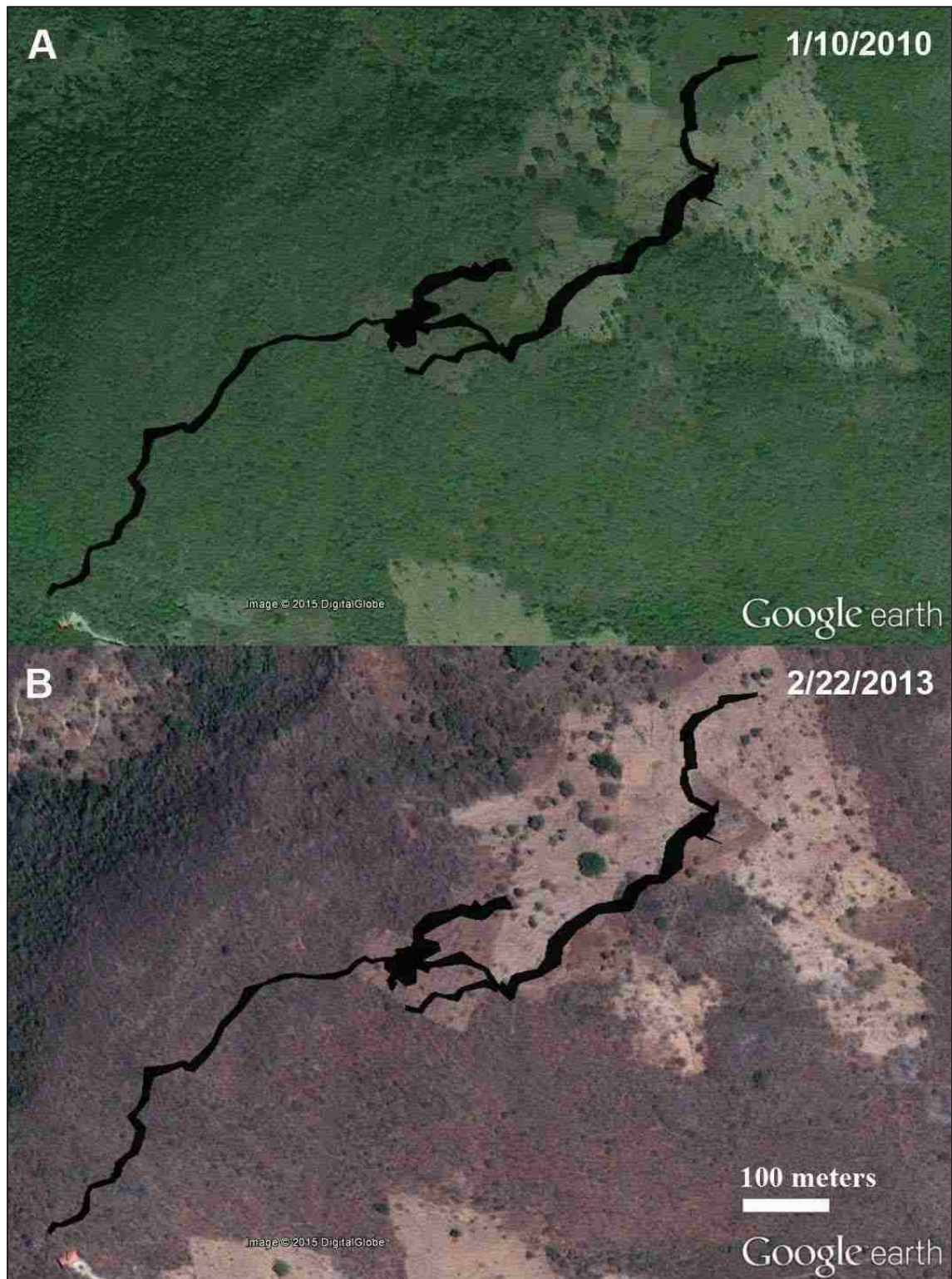


Figure 2 Satellite imagery of the surface vegetation above Juxtlahuaca Cave (black) near the end of the (A) wet season (1/10/2010) and the (B) middle of the dry season (2/22/2013). Both images show sections of land above the cave that have been cleared for agricultural use. Images provided by Google Earth and DigitalGlobe (2015).

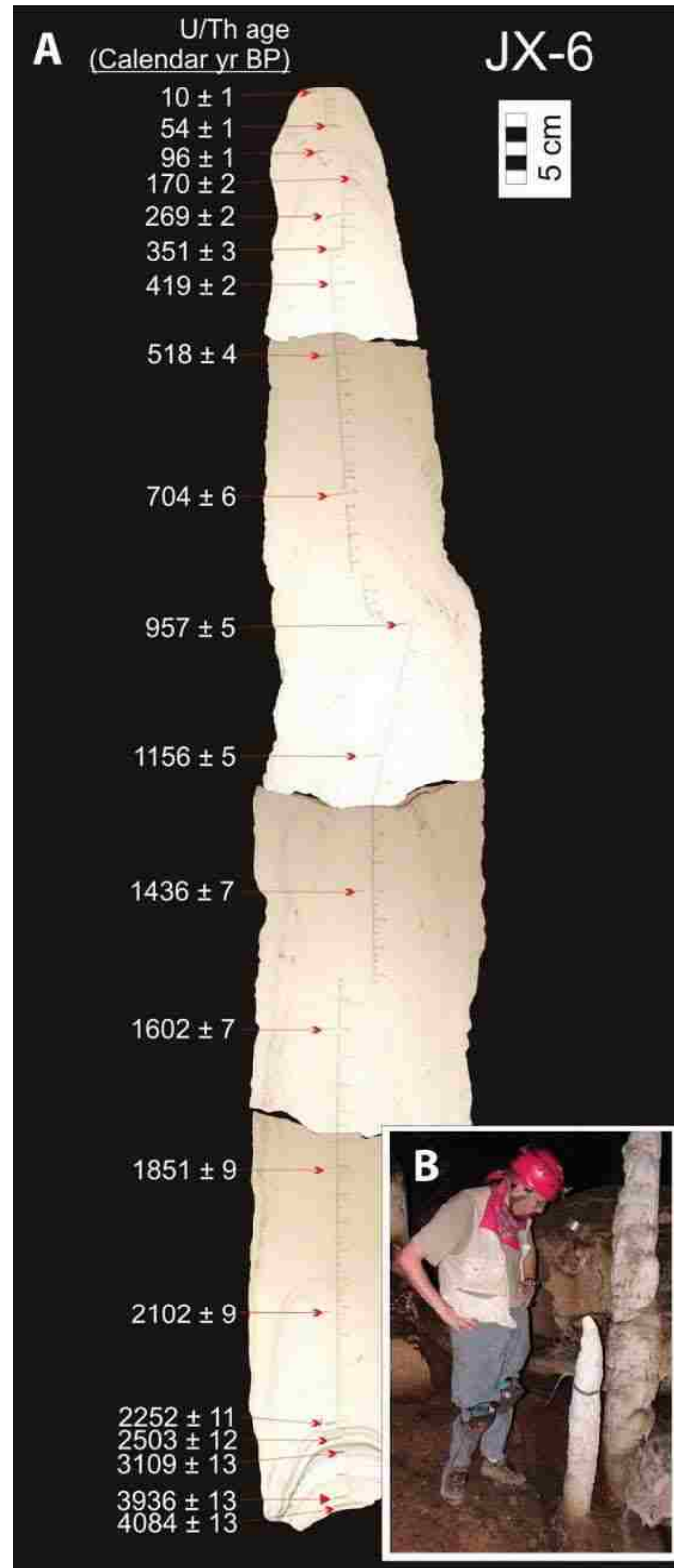


Figure 3 (A) Picture of JX-6 showing the growth axis and locations of the U/Th ages (yr BP refers to years before 2010). (B) Picture of JX-6 sampling location within the La Sorpresa passage of Juxtlahuaca Cave. Figures modified from Lachniet et al. (2012a).

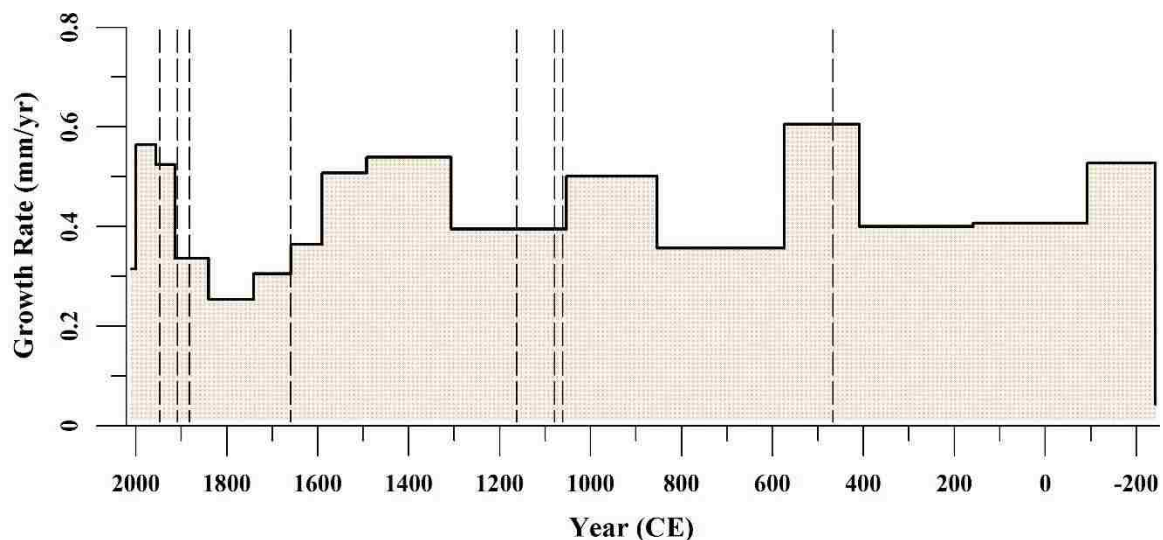


Figure 4 Graph showing the growth rate of JX-6 between 240 BCE to 2010 CE. Growth rates determined from the 16 U-series ages (Lachniet et al., 2012a) bracketing this time interval. Vertical dashed lines represent minor shifts in the drip axis of JX-6.

2.2 Previous [U] Studies

Recent work has led to dissimilar and conflicting interpretations on the mechanisms that control the variations of [U] in speleothems. The results of this study will be compared to the three most relevant previous studies involving [U] in speleothems (Hellstrom & McCulloch, 2000; Johnson et al., 2006; Treble et al., 2003). The results of this study will also be compared to a study involving the mobility of U in groundwater (Langmuir, 1978), which directly relates to [U] in cave dripwaters. For the three speleothem studies, time scales and sampling resolutions differ greatly due to the varying ages and growth rates of the different samples. Methods of analyzing trace element concentrations and dating techniques also differ slightly for similar reasons. However, three of these studies show that U is incorporated into the speleothem through precipitation of CaCO_3 from cave dripwaters. They also suggest that the U in those dripwaters is mainly sourced from the overlying soils and transported by varying amounts of rainfall through the epikarst to the cave. The main difference between these studies is their interpretations on the mechanisms affecting [U] as it is transported from the soils to the cave. These hypotheses include:

- 1.) *Oxidation Control Hypothesis*: An increase in biological activity in the soils overlying a cave will cause a decrease in the amount of U being oxidized to its more mobile hexavalent state [U(VI)], thus, causing lower [U] in water flushed through the soils and eventually in cave dripwaters (Hellstrom & McCulloch, 2000). If the variations in [U] of JX-6 are controlled by a decrease in oxidation due to an increase in biological activity in the soils, then [U] should decrease during periods of greater biological activity.
- 2.) *Prior Calcite Precipitation Control Hypothesis*: U is adsorbed onto mineral surfaces during prior calcite precipitation (PCP) in the epikarst, therefore, decreasing the amount of [U] in cave drip-waters during drier periods (Johnson et al., 2006). If the variations in [U] of JX-6 are controlled by PCP, then [U] would be expected to decrease during drier periods.
- 3.) *Phosphorus Control Hypothesis*: An increase in [P] in soils, possibly due to seasonal decay of vegetation, will increase the mobility and transport of U within these soils. Therefore, increasing the amount of [U] in cave drip-waters with increasing seasonal decay of vegetation (Treble et al., 2003). If the variations in [U] of JX-6 are controlled by the amount of P in the soil, then [U] would increase in periods of higher vegetation growth and decay.
- 4.) *pCO₂ Control Hypothesis*: Increasing pCO₂ will increase the solubility of U in groundwater (Langmuir, 1978), and therefore increase [U] of cave dripwaters, recorded in speleothem CaCO₃. If the variations in [U] of JX-6 are controlled by variations in the pCO₂ of overlying soils, then [U] should increase during periods of increased plant respiration, assumed to be the main driver of soil pCO₂.

In order to better understand how the new trace element data from JX-6 compares to the previous speleothem studies, a review of the results and interpretations of the three studies is outlined below.

2.2.1 Oxidation Control Hypothesis

Hellstrom & McCulloch (2000) collected a core (MD3) from a flowstone in Nettlebed Cave, located in the northern part of New Zealand's South Island. U-series analysis of core MD3 suggests that it grew continuously for the last 31,000 cal yr BP. U concentrations exhibit a general decrease over this time from ~150 ppm to ~50 ppm, with an abrupt decrease in these values around the last glacial maximum (LGM) at ~18,000 cal yr BP (Figure 5). Hellstrom & McCulloch (2000) interpret the cause of this abrupt decrease in [U] to be the result of increased biological activity following the LGM. They claim that increased biological activity produces less oxidizing conditions in the soils overlying a cave, leading to less oxidation of U to its more soluble hexavalent state [U(VI)]. This would lead to a decrease in the amount of U transported from the soil to the cave, and therefore a decrease in the amount of U present in speleothem deposits. They claim this interpretation is supported by the shift in $\delta^{13}\text{C}$ to more negative values around the same time (Figure 6), which could also be caused by an increase in biological activity.

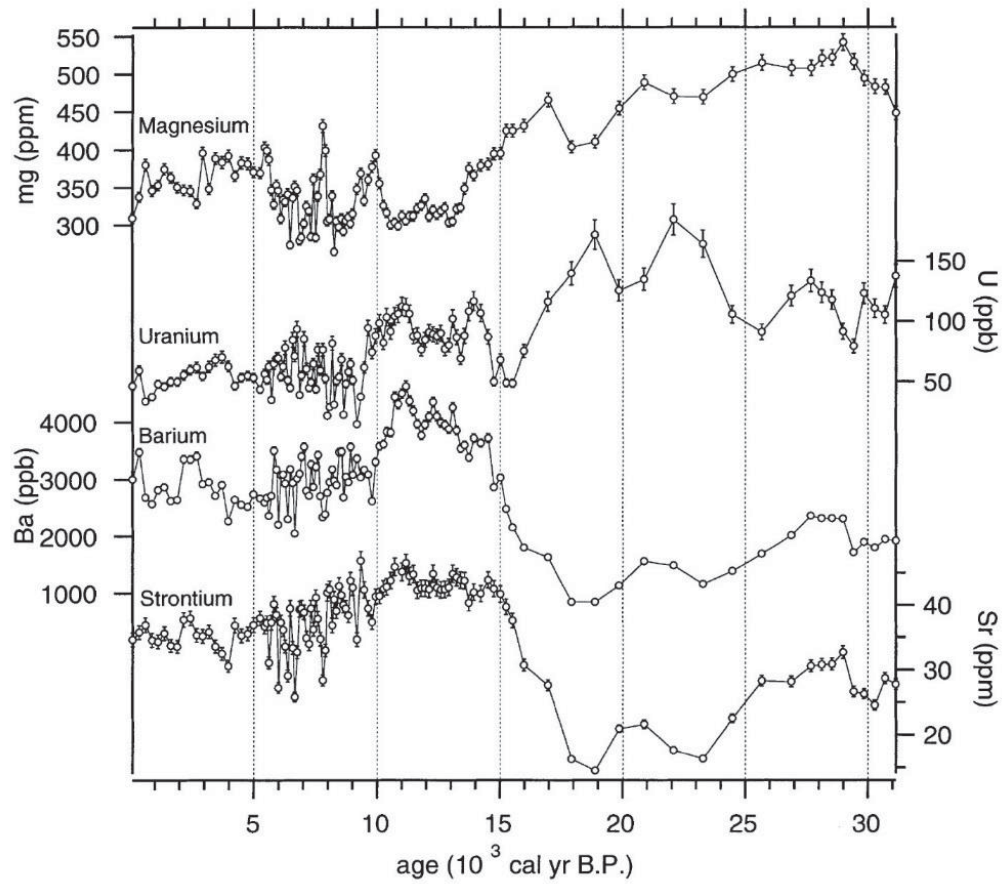


Figure 5 Trace element concentrations from core MD3 versus linearly interpolated ages from U-series analysis. Figure from Hellstrom & McCulloch (2000).

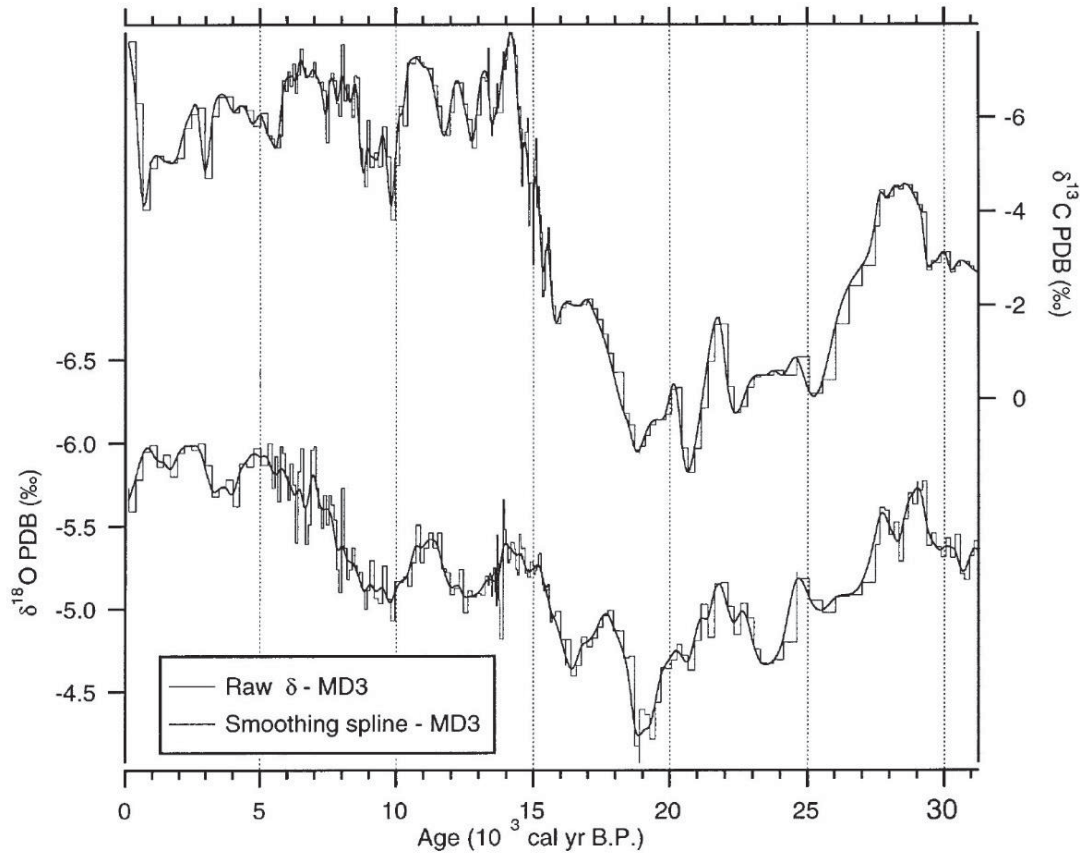


Figure 6 Stable isotope values from core MD3 versus linearly interpolated ages calculated from U-series analysis. Figure from Hellstrom et al. (1998).

2.2.2 Prior Calcite Precipitation Control Hypothesis

Johnson et al. (2006) measured trace element to calcium ratios (Tr/Ca) in a stalagmite (HS-4) from Heshang Cave in southern China. The U/Ca ratios of the HS-4 segment show a negative correlation to Mg/Ca, Sr/Ca, Ba/Ca, and $\delta^{13}\text{C}$ values ($r = -0.5$ to -0.6). Higher [U] correspond to darker growth bands, whereas higher Mg, Sr, Ba, and $\delta^{13}\text{C}$ values correspond to lighter growth bands within the HS-4 segment (Figure 7). Sixteen annual cycles were interpreted from troughs in the Mg/Ca data by Johnson et al. (2006). In an attempt to better understand these chemical cycles on a sub-annual scale, cycles 7-12 were partitioned into 12 equidistant points using linear interpolation. These points, which they refer to as “growth increments,” were then averaged to

create composite annual cycles (Figure 8). Johnson et al. (2006) interpreted the spike in $\delta^{18}\text{O}$ to more positive values at increment 5 to represent the beginning of monsoonal rains in the month of May. This increased rainfall in May is thought to force the “heavier” winter rains through the epikarst, causing the spike in $\delta^{18}\text{O}$ values. However, they state that the other growth increments are not representative of single months in a year due to varying growth rates of HS-4.

Assuming that growth increment 5 represents the beginning of monsoonal rainfall, the composite annual cycles suggest that Mg, Sr, and Ba are at their lowest concentrations during the wet season. In contrast, [U] are at their highest during this time. Johnson et al. (2006) propose that PCP in the epikarst is the cause of these relationships. During the dry season, groundwater flowing from the soil (high $p\text{CO}_2$ levels) to the epikarst (lower $p\text{CO}_2$ levels) would cause the precipitation of CaCO_3 due to degassing of CO_2 . During this process, ^{12}C is preferentially degassed over ^{13}C , increasing the $\delta^{13}\text{C}$ values of the groundwater. Calcium is also preferentially removed from groundwater over Mg, Sr, and Ba due to how these elements partition into calcite (Huang & Fairchild, 2001). Therefore, during the dry season, increased PCP would cause $\delta^{13}\text{C}$ values and Tr/Ca ratios in cave drip-waters to increase. Johnson et al. (2006) suggest that during PCP, U is ‘scavenged’ from the groundwater onto mineral surfaces. Through this mechanism, [U] in speleothems further down the flow path would decrease during drier periods and increase during wetter periods. Increased PCP would also lead to increasing $\delta^{13}\text{C}$, Mg/Ca, Sr/Ca, and Ba/Ca during drier periods. This interpretation is supported by the negative correlation of $\delta^{13}\text{C}$, Mg/Ca, Sr/Ca, and Ba/Ca, to the U/Ca ratios of HS-4.

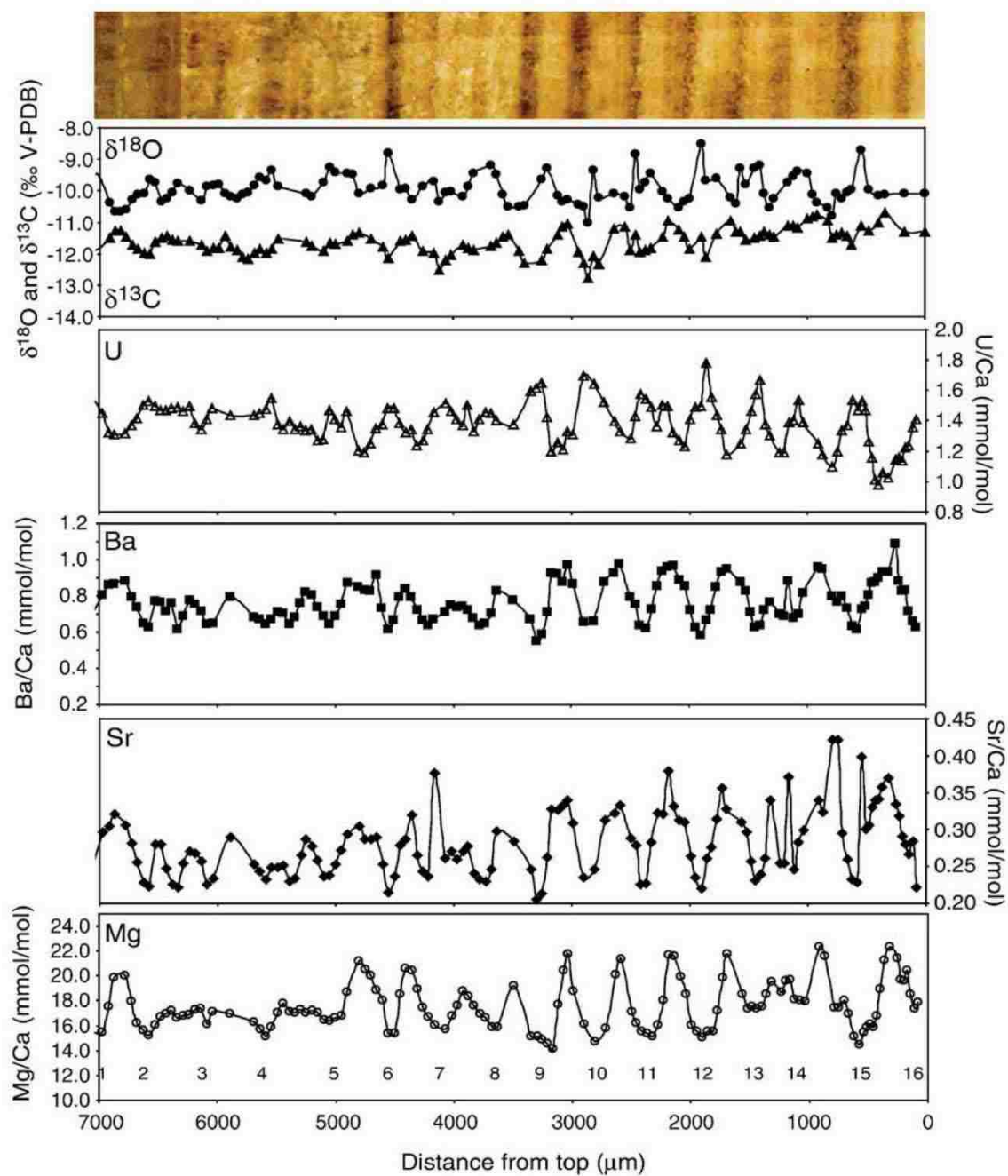


Figure 7 Image of light-dark bands of HS-4 (top) next to trace element concentrations and isotope values plotted against distance from the top of HS-4 (in μm). Numbers below Mg troughs indicate interpreted annual cycles (16 total cycles). Composite annual cycles were created from cycles 7-12. Figure from Johnson et al. (2006).

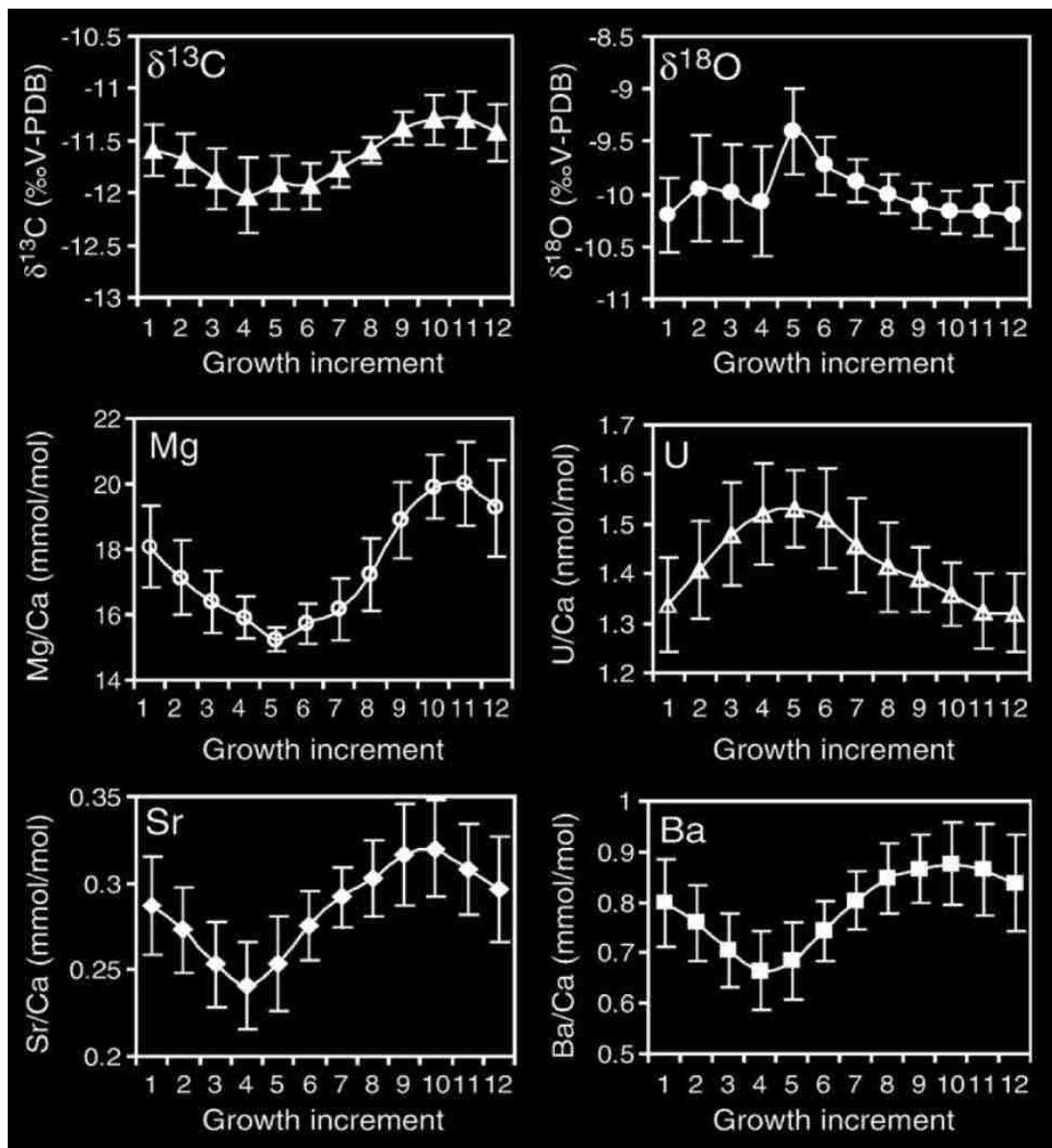


Figure 8 Cycles 7-12 from Figure 7 were partitioned into 12 equidistant points using linear interpolation and then averaged to create composite annual cycles for the trace element and stable isotope values of HS-4. Growth increment 5 is interpreted as representing the month of May, however, other growth increments are not representative of single months in a year due to varying growth rates of HS-4. Figure from Johnson et al. (2006).

2.2.3 Phosphorus Control Hypothesis

Treble et al. (2003) measured high-resolution trace element concentrations from a 33-mm-tall stalagmite (MND-S1) that grew between 1911 to 1992 CE on a manmade boardwalk in Moondyne Cave in southwestern Australia. Stalagmite MND-S1 displayed near annual cycles in trace element concentrations over its 80 years of growth (84 ± 1.3 cycles for Ba). U concentrations were positively correlated to [Ba] ($r = 0.92$), [Sr] ($r = 0.72$), and [P] ($r = 0.60$), and negatively correlated to [Mg] ($r = -0.80$). Each cycle, based on well-defined troughs in the Ba data, was partitioned into 12 equidistant points using linear interpolation. These 12 points were then averaged to create composite annual cycles and compared to averaged monthly rainfall data (Figure 9). These composite annual cycles indicated that U, Sr, Ba, and P reach maximum concentrations during the wet summer months. Mg appears to reach maximum concentrations during the drier winter months. Two distinct periods are specified during the growth of MND-S1: a wetter period from 1911-1964 (Episode I); and a drier period from 1965-1992 (Episode II) (Figure 10). U, Ba, and P exhibit a general decrease in maximum concentrations from Episode I – Episode II. Treble et al. (2003) propose that an increase in [P], possibly due to the seasonal decay of vegetation, may increase the mobility and transport of U in soils. They suggest that increased [P] may lead to the formation of more uranyl phosphate complexes, increasing [U] in the groundwater. This interpretation is supported by the positive correlation between [U] and [P], and by the general decrease in both concentrations from the wetter Episode I to the drier Episode II. This assumes that more vegetation will grow and decay during wetter years, increasing [P], and therefore [U] in speleothems.

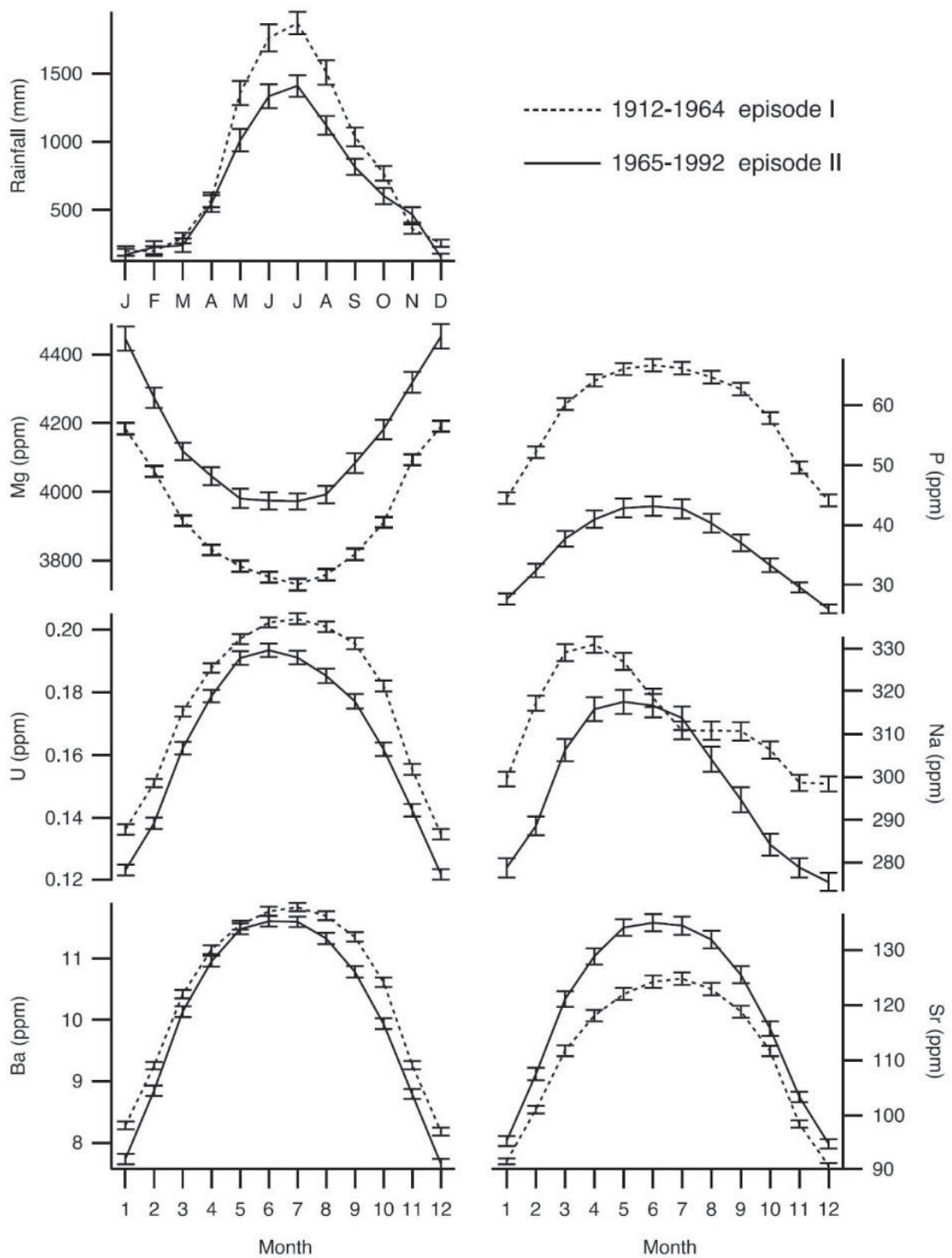


Figure 9 Annual cycles, based on Ba troughs, were portioned into 12 equidistant points and then averaged to create composite annual cycles for the trace element concentrations of MND-S1. Treble et al. (2003) state that each 'Month' increment may not represent an actual month of the year due to varying growth rates of MND-S1. Data are separated to display the change from Episode I to Episode II. Figure from Treble et al. (2003).

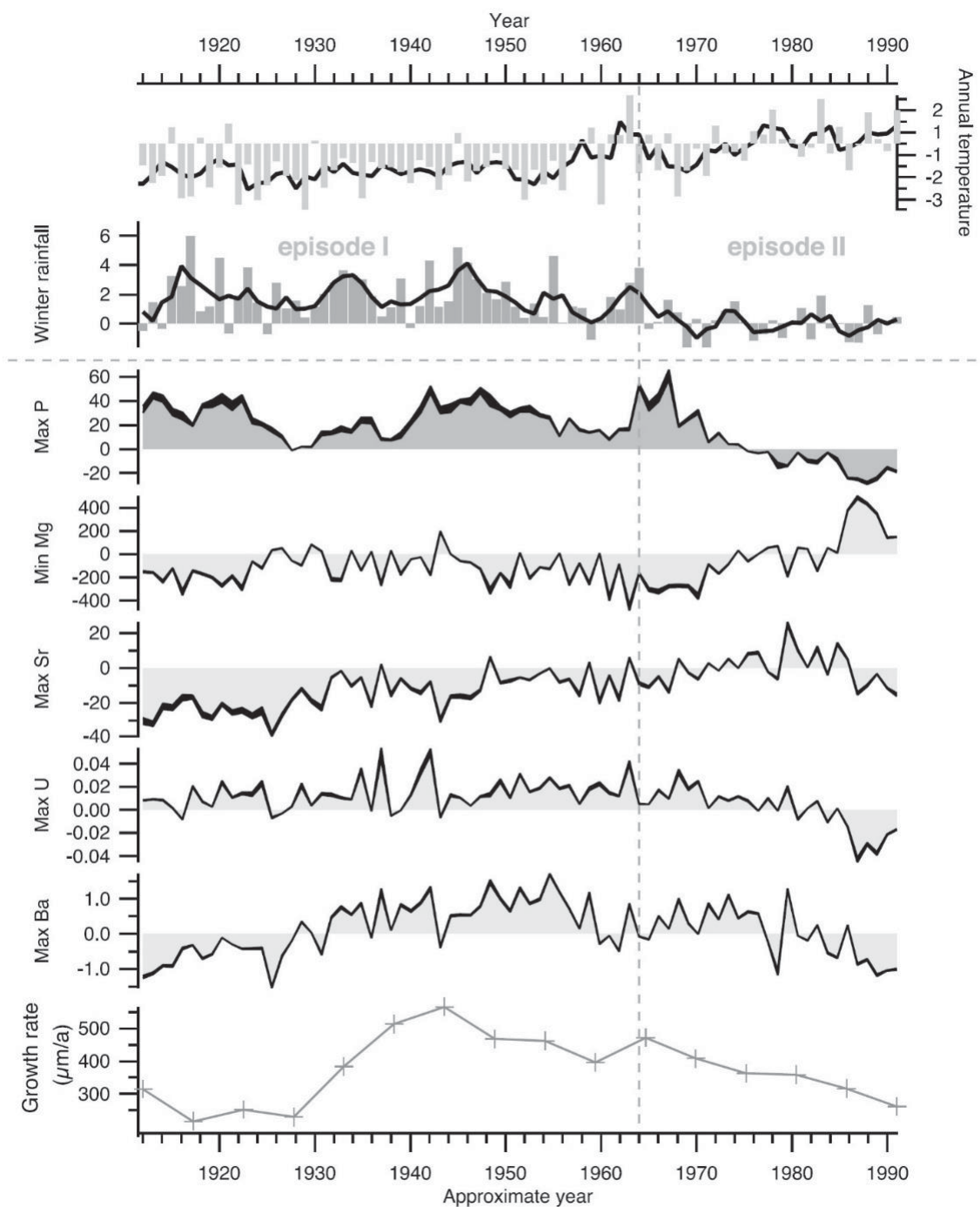


Figure 10 Maximum trace element concentrations within each cycle (minimum for Mg) plotted next to winter rainfall and annual temperature anomalies (top), and growth rate (bottom). Trace element concentrations are normalized to the 1965-1992 mean. Figure from Treble et al. (2003).

2.2.4 $p\text{CO}_2$ Control Hypothesis

Langmuir (1978) assessed the effect of Eh, pH, and $p\text{CO}_2$ in ground waters on 42 dissolved U species. Their compiled data suggest that increases in $p\text{CO}_2$ will increase the solubility of uranyl minerals, and therefore increase the [U] dissolved in groundwater. This implies that an increase in the $p\text{CO}_2$ in soils, may increase the dissolved [U] within the water of that soil, and therefore cave dripwaters.

3. Methods

The stable isotope values ($\delta^{18}\text{O}$ and $\delta^{13}\text{C}$) from Lachniet et al. (2012a) were measured at the Las Vegas Isotope Science Lab (LVIS) at the University of Nevada, Las Vegas (UNLV). Samples were micro milled along the growth axis of JX-6 at a 0.25 mm resolution for the top 80 mm, and at a 1 mm resolution for the remaining 910 mm. Powders for $\delta^{18}\text{O}$ and $\delta^{13}\text{C}$ were reacted with phosphoric acid at 70 °C, and dripwater $\delta^{18}\text{O}$ was measured on a TC/EA device. Results were reported in ‰ relative to Vienna Pee Dee Belemnite (VPDB) and Vienna Standard Mean Ocean Water (VSMOW) standards (Lachniet et al., 2012a).

Trace element concentrations and U-series isotope values were measured at the Radiogenic Isotope Geochemistry lab at the University of New Mexico. Twenty U-series ages were determined from 50-200 mg powdered samples that were dissolved in nitric acid, spiked with ^{229}Th - ^{233}U - ^{236}U , and analyzed on a Thermo Neptune multi-collector inductively coupled plasma mass spectrometer (MC ICP-MS) (Lachniet et al., 2012a). Trace element concentrations (^{24}Mg , ^{25}Mg , ^{84}Sr , ^{88}Sr , ^{137}Ba , and ^{238}U) were measured on a Thermo X-series quadrupole inductively coupled plasma mass spectrometer (Q-ICP-MS). A 2 mm wide drill bit was used to mill ~10 mg samples along the growth axis of the stalagmite, creating “trenches” 1.5-4 mm deep (Figure 11). Differences in “trench” depth were due to changes in porosity, which influenced powder yield that could be drilled at a given sampling interval. Samples were drilled at 1 mm intervals for the top 80 mm of JX-6, and at 2 mm intervals for the remaining 910 mm of the stalagmite, resulting in 535 total samples. It was decided that higher resolution data for the top 80 mm would be beneficial to the study as there is instrumental rainfall data within that respective time interval (1880 – 2010 CE). After each sample was milled out and placed in a small plastic vial, the stalagmite surface was cleaned with compressed air to remove powder from previous samples. Before dissolving samples in nitric acid, 125 ml bottles were rinsed with 6 N HCl solution once, then twice with ultra-pure water to limit contamination. A Mettler Toledo AT261 Delta Range Analytical Balance was used to weigh each

sample. Each bottle and vial was shot with an anti-static gun before weighing to increase measurement accuracy. Samples were weighed in small plastic vials, the scale was zeroed, and the samples were transferred into 125 ml bottles. The empty plastic vials were then weighed again to acquire the weight of each sample. Approximately 3–4 drops of 7 N nitric acid were added to each bottle to ensure complete dissolution. Samples were then diluted with ~100 ml of 3% nitric acid spiked with 10 ppb indium to reach dilution-factors between 2,000 and 10,000. Full bottles were then weighed on the balance again to get a final diluted sample weight. Dilution factors were calculated by subtracting empty bottle weights from the full diluted sample bottle weights and then dividing by the weight of the powdered sample.

Six different standards were created using *Inorganic Ventures IV-ICPMS-71A* solution. This standard contains 71 elements at a 10 µg/ml concentration in a matrix of 2% nitric acid. Standards were diluted with 3% nitric acid to create six different standards with concentrations of 500, 200, 100, 50, 20, and 5 ppb. Blank solutions were also created consisting only of 3% nitric acid spiked with 10 ppb indium. Each run on the ICP-MS started with one blank, followed by the six standards, two more blanks, and then 30 samples. Runs ended with two blanks and 3 standards (500, 200, and 20 ppb) to account for instrumental drift.

All correlations and interpolations were completed in Microsoft Excel 2013. Isotopic values from Lachniet et al. (2012a) were averaged within trace element intervals to permit correlations between different sampling resolutions. Isotope and trace element concentrations were interpolated to single yearly values to perform correlations between annual rainfall and temperature measurements (1880 – 2010 CE). Rainfall at the surface, and therefore isotope and trace element values, may take several years to travel through the ~160 m of carbonate bedrock before being precipitated at the tip of the stalagmite. Various yearly lags were applied to stable isotope values in correlations to instrumental rainfall and temperature data to account for this travel time. During this time, mixing of groundwater from multiple years/events may also occur, possibly leading to muted signals from stable isotope or trace element concentrations. Various running averages were also

used in correlations to account for this potential mixing in the vadose zone. The instrumental rainfall and temperature data used in correlations comprises the last 130 years (1880 – 2010 CE). A maximum of 13-year running averages were used to calculate correlations between stable isotope values and instrumental data to prevent artificially strong correlations. Logarithmic scales were also used in correlations to account for finer scale variability in trace element concentrations that may have been overlooked using absolute values. This was based on trace element concentrations exhibiting log normal distributions over specific time intervals (See *Appendix*, Figures A1 – A4).

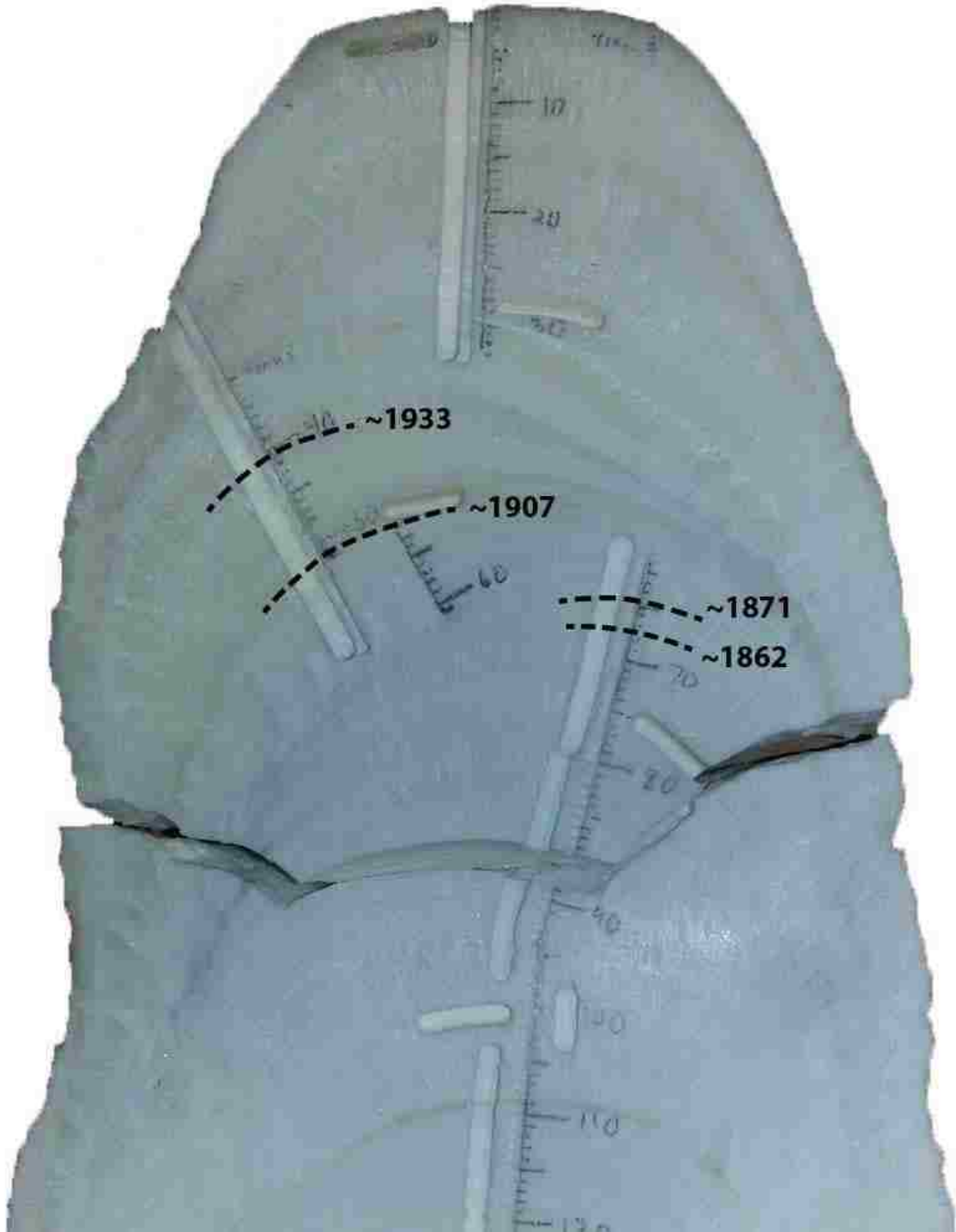


Figure 11 Picture of the upper 120 mm of JX-6 showing locations of milled trenches along the growth axis, drawn in pencil. Specific growth layers indicated by black dashed lines represent approximate ages (years CE) of anomalous spikes in trace element concentrations discussed in *Section 5.1*.

4. Results

4.1 Stable Isotopes

Using the twenty U-series ages and 1,230 stable isotope measurements from JX-6, Lachniet et al. (2012a) created a 2,400 year time series containing sub-annual resolution over the upper 80 mm (1820 – 2010 CE) and stable isotope values every 2-3 years for the subsequent 900 mm (240 BCE to 1820 CE) (Figure 12). The coarsest age resolution occurs between 980 mm and the base of JX-6 (pre-240 BCE). Due to the slow growth rate and high variability in trace element concentrations, this section is assumed to contain micro-hiatuses and was not used in the correlations of this study.

Over the upper 980 mm the $\delta^{18}\text{O}$ values fluctuate by about 1.5‰ across the time series, with a minimum value of -9.4‰ and a maximum value of -6.8‰ VPDB (Figure 12). Lachniet et al. (2012a) interpolated the sub annual $\delta^{18}\text{O}$ values to annual resolution. These interpolated values were then correlated to annual wet season (May – November) rainfall measurements from Tacubaya Station in Mexico City (1880 – 2010 CE). The best correlation of $\delta^{18}\text{O}$ values and wet season rainfall was found using 5-year running averages from 1880 – 1988 with a 9 year lag in the $\delta^{18}\text{O}$ values ($r = -0.89$). The 9 year lag implies an average of ~9 years for rainfall to travel through the ~160 m of carbonate bedrock before reaching the cave. Rainfall measurements after 1988 were removed from this correlation due to the possibility of recent anthropogenic effects altering the data (Jauregui, 1990). Including this most recent rainfall data (1989 to 2008 CE) still returns a strong correlation ($r = -0.76$) with an 8 year lag in the $\delta^{18}\text{O}$ values (Figure 13).

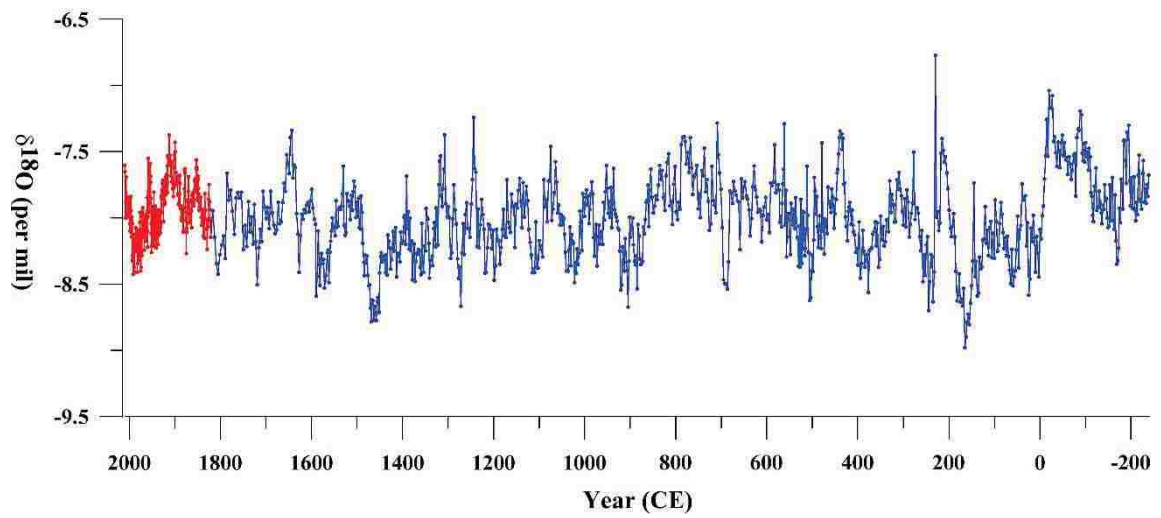


Figure 12 Graph showing $\delta^{18}\text{O}$ values of JX-6 between 240 BCE to 2010 CE. Higher resolution data (0.25 mm) shown in red, lower resolution data (1 mm) shown in blue. Data from Lachniet et al. (2012a).

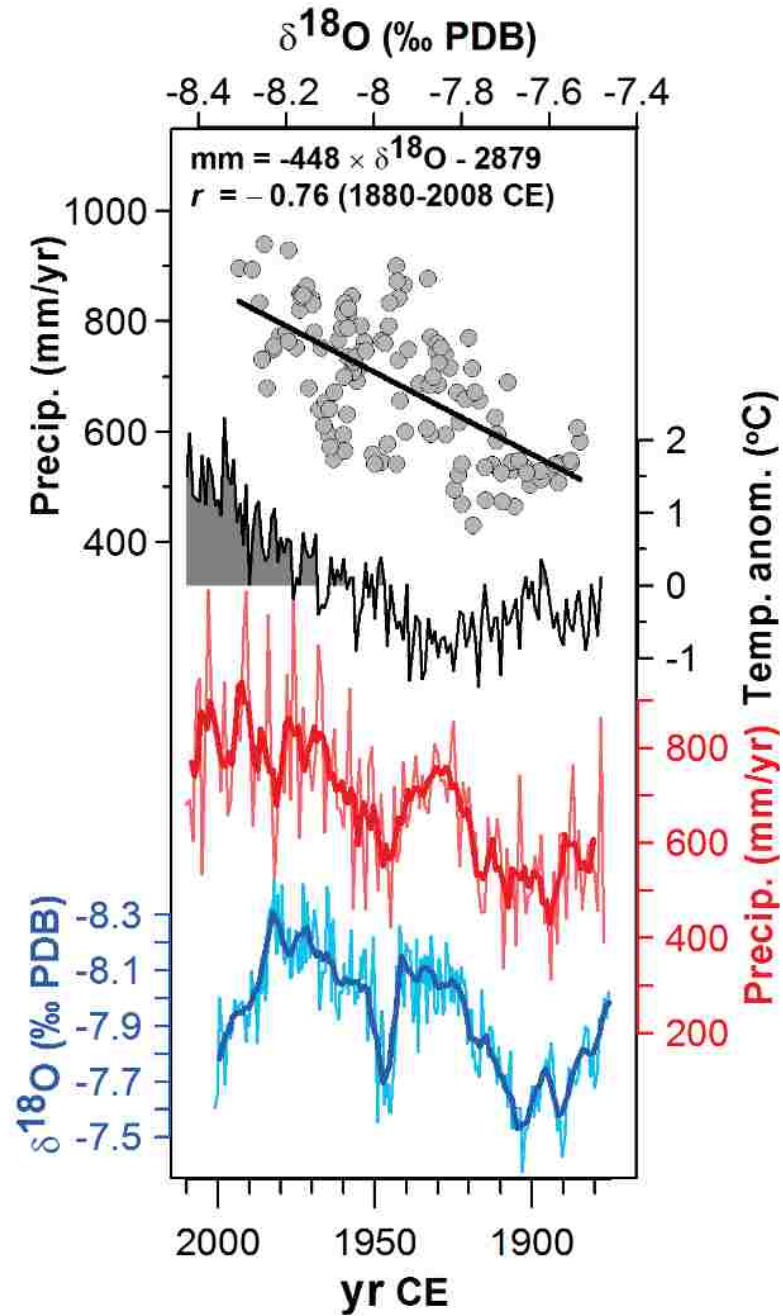


Figure 13 Correlation between wet season rainfall and $\delta^{18}\text{O}$ values of JX-6 (9-year lag) using 5-year running averages (top). Relationships between temperature anomalies (black) and wet season rainfall (red) from Tacubaya Station in Mexico City, and $\delta^{18}\text{O}$ values of JX-6 (blue). Thick lines in precipitation and $\delta^{18}\text{O}$ graphs represent 5-year running averages. Figure from Lachniet et al. (2012a).

The $\delta^{13}\text{C}$ values of JX-6 range from -8.95‰ to -2.86‰ VPDB (Figure 14) between 240 BCE to 2010 CE. These data have not yet been published, and are considered here for the first time. $\delta^{13}\text{C}$ values are characterized by a sharp decrease from ~1907 (-3.05‰) to 2007 CE (-8.95‰). $\delta^{13}\text{C}$ exhibits a strong negative correlation with wet season (MJJASON) rainfall ($r = -0.65$) and annual median temperatures ($r = -0.62$) between 1880 – 2008 CE (Tables 1 and 2). The strength of these correlations is a result of all three data sets displaying similar linear trends within the specified time interval (Figure 15). Detrending these data sets considerably decreases the correlation between $\delta^{13}\text{C}$ and wet season rainfall ($r = -0.22$) (Table 3), and changes the correlation between $\delta^{13}\text{C}$ and median temperature from negative to positive ($r = 0.22$) (Table 4; Figure 16). The correlations between detrended $\delta^{13}\text{C}$ and wet season rainfall weaken with an increasing lag in $\delta^{13}\text{C}$ values ($r = -0.06$ with a 9 year lag) and strengthen with an increasing running average ($r = -0.675$ with a 13-year running average) (Table 3). The correlations between $\delta^{13}\text{C}$ and median temperatures also weaken with an increasing lag in $\delta^{13}\text{C}$ values ($r = 0.11$ with a 9 year lag) and strengthen with an increasing running average ($r = 0.45$ with a 13-year running average) (Table 4). $\delta^{13}\text{C}$ also exhibits a positive correlation to $\delta^{18}\text{O}$ ($r = 0.45$) and a negative correlation to [U] ($r = -0.29$) and the $\log(^{238}\text{U})$ ($r = -0.40$) between 240 BCE to 2010 CE when no running averages are applied (Table 5). Removing the most recent data (1800 – 2010 CE) increases the relationship between $\delta^{13}\text{C}$ and $\delta^{18}\text{O}$ ($r = -0.54$) and between $\delta^{13}\text{C}$ and [U] ($r = -0.36$) (Table 6; Figure 17). All correlations involving $\delta^{13}\text{C}$ with a p -value > 0.05 are considered insignificant (Tables A1 – A6).

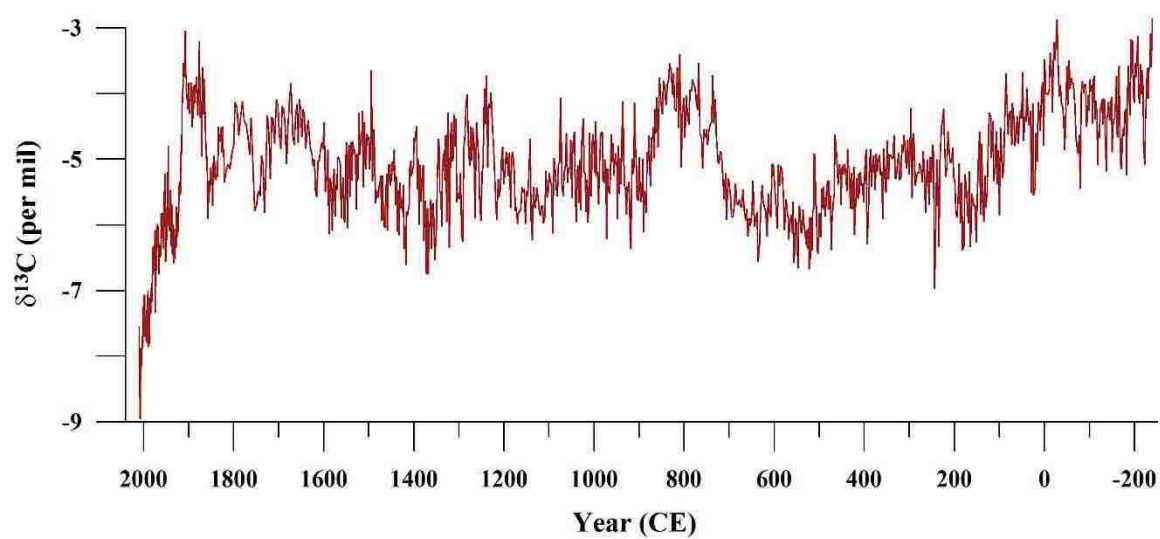


Figure 14 $\delta^{13}\text{C}$ values of JX-6 between 240 BCE to 2010 CE in per mil VPDB.

Table 1 Correlation coefficients (r) for yearly interpolated $\delta^{13}\text{C}$ of JX-6 and wet season rainfall (May – November) with various running averages and yearly lags in $\delta^{13}\text{C}$ values between 1880 to 2010 CE. Bold values indicate the strongest correlations.

Correlations between $\delta^{13}\text{C}$ and Wet Season Rainfall (1880 – 2010 CE)										
Running Average	Lag in $\delta^{13}\text{C}$ (years)									
	No Lag	1	2	3	4	5	6	7	8	9
Original Data	-0.65	-0.64	-0.66	-0.63	-0.64	-0.63	-0.60	-0.61	-0.62	-0.60
3-year	-0.84	-0.84	-0.85	-0.84	-0.83	-0.81	-0.80	-0.79	-0.79	-0.77
5-year	-0.89	-0.89	-0.89	-0.89	-0.88	-0.87	-0.86	-0.85	-0.83	-0.81
7-year	-0.92	-0.92	-0.92	-0.92	-0.91	-0.90	-0.89	-0.88	-0.86	-0.84
9-year	-0.94	-0.94	-0.93	-0.93	-0.92	-0.91	-0.90	-0.88	-0.87	-0.84
11-year	-0.95	-0.95	-0.94	-0.94	-0.93	-0.92	-0.90	-0.89	-0.87	-0.85
13-year	-0.95	-0.95	-0.95	-0.94	-0.93	-0.92	-0.91	-0.89	-0.88	-0.86

Table 2 Correlation coefficients (r) for yearly interpolated $\delta^{13}\text{C}$ of JX-6 and annual median temperature with various running averages and yearly lags in $\delta^{13}\text{C}$ values between 1880 to 2010 CE. Bold values indicate the strongest correlations.

Correlations between $\delta^{13}\text{C}$ and Median Temperature (1880 – 2010 CE)										
Running Average	Lag in $\delta^{13}\text{C}$ (years)									
	No Lag	1	2	3	4	5	6	7	8	9
Original Data	-0.62	-0.62	-0.63	-0.62	-0.62	-0.63	-0.63	-0.64	-0.63	-0.65
3-year	-0.67	-0.67	-0.67	-0.67	-0.67	-0.68	-0.68	-0.69	-0.69	-0.71
5-year	-0.68	-0.68	-0.68	-0.68	-0.68	-0.69	-0.69	-0.70	-0.71	-0.71
7-year	-0.68	-0.68	-0.68	-0.68	-0.69	-0.69	-0.70	-0.70	-0.71	-0.71
9-year	-0.68	-0.68	-0.68	-0.68	-0.69	-0.69	-0.70	-0.70	-0.71	-0.71
11-year	-0.68	-0.68	-0.68	-0.68	-0.69	-0.69	-0.69	-0.70	-0.71	-0.72
13-year	-0.67	-0.68	-0.68	-0.68	-0.68	-0.69	-0.69	-0.70	-0.71	-0.72

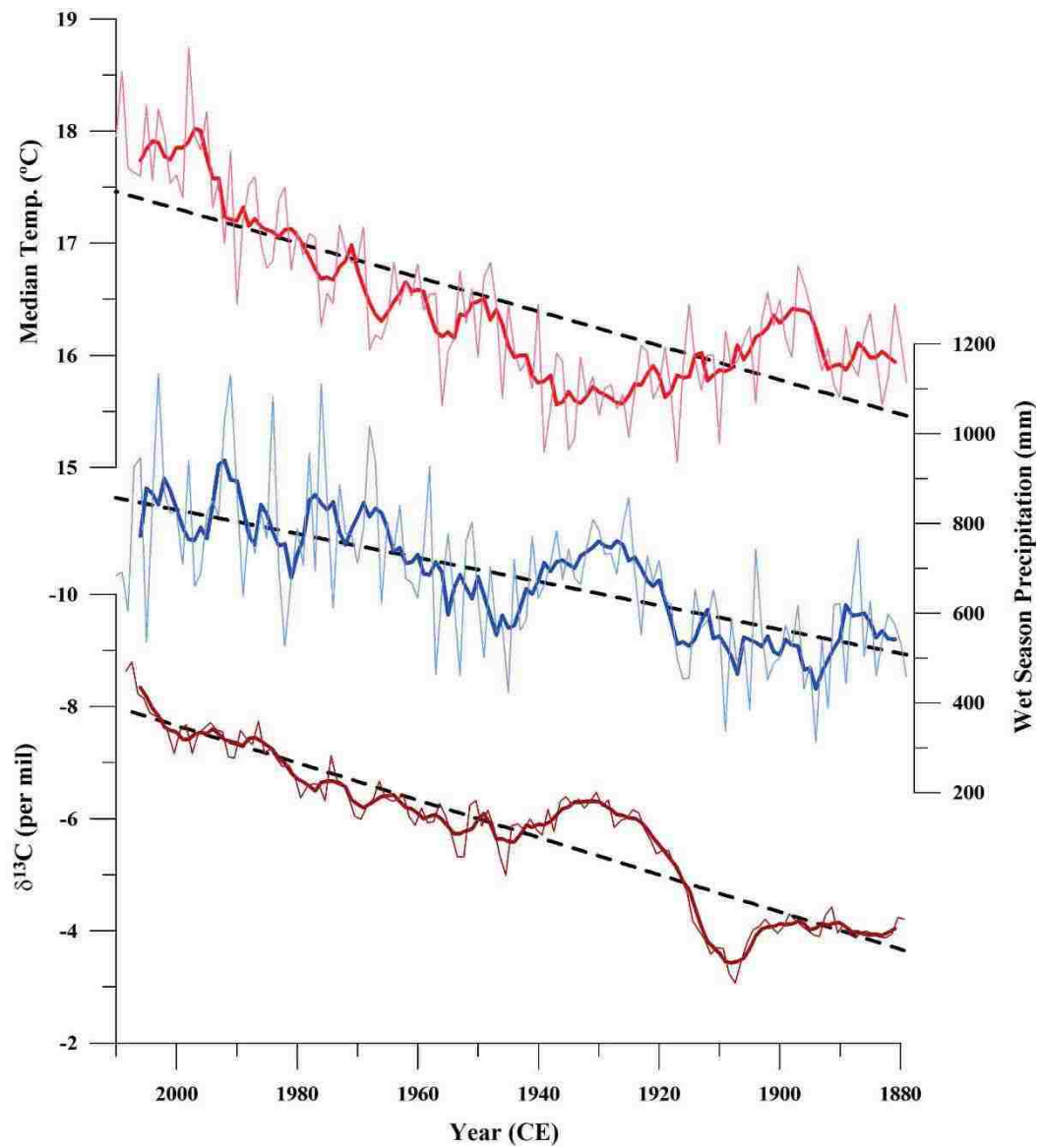


Figure 15 Annual median temperature (red), wet season rainfall totals (blue), and yearly interpolated $\delta^{13}\text{C}$ values (brown) from JX-6 between 1880 to 2010 CE. Thick lines represent 5-year running averages and dashed lines represent linear trends. Instrumental rainfall and temperature data collected from Tacubaya Station in Mexico City.

Table 3 Correlation coefficients (r) for detrended yearly interpolated $\delta^{13}\text{C}$ of JX-6 and detrended wet season rainfall (May – November) with various running averages and yearly lags in $\delta^{13}\text{C}$ values between 1880 to 2010 CE. Bold value indicates the strongest correlation.

Correlations between Detrended $\delta^{13}\text{C}$ and Wet Season Rainfall (1880 – 2010 CE)										
Running Averages	Lag in $\delta^{13}\text{C}$ (years)									
	No Lag	1	2	3	4	5	6	7	8	9
Original Data	-0.22	-0.23	-0.28	-0.18	-0.23	-0.19	-0.12	-0.13	-0.19	-0.06
3-year	-0.41	-0.44	-0.44	-0.41	-0.38	-0.32	-0.28	-0.23	-0.18	-0.10
5-year	-0.51	-0.52	-0.52	-0.50	-0.47	-0.41	-0.35	-0.28	-0.20	-0.10
7-year	-0.60	-0.60	-0.59	-0.56	-0.52	-0.47	-0.39	-0.31	-0.21	-0.10
9-year	-0.63	-0.63	-0.62	-0.58	-0.54	-0.47	-0.40	-0.31	-0.21	-0.10
11-year	-0.66	-0.65	-0.63	-0.59	-0.54	-0.47	-0.39	-0.30	-0.21	-0.10
13-year	-0.67	-0.66	-0.64	-0.59	-0.54	-0.47	-0.39	-0.30	-0.20	-0.10

Table 4 Correlation coefficients (r) for detrended yearly interpolated $\delta^{13}\text{C}$ of JX-6 and detrended annual median temperatures with various running averages and yearly lags in $\delta^{13}\text{C}$ values between 1880 to 2010 CE. Bold values indicate the strongest correlations.

Correlations between Detrended $\delta^{13}\text{C}$ and Median Temperature (1880 – 2010 CE)										
Running Averages	Lag in $\delta^{13}\text{C}$ (years)									
	No Lag	1	2	3	4	5	6	7	8	9
Original Data	0.22	0.22	0.22	0.23	0.23	0.19	0.19	0.18	0.23	0.11
3-year	0.28	0.31	0.32	0.31	0.29	0.27	0.26	0.25	0.22	0.17
5-year	0.33	0.34	0.35	0.34	0.33	0.31	0.29	0.27	0.24	0.20
7-year	0.36	0.37	0.37	0.37	0.35	0.33	0.31	0.28	0.25	0.22
9-year	0.40	0.40	0.40	0.39	0.37	0.35	0.33	0.30	0.27	0.24
11-year	0.42	0.42	0.42	0.40	0.39	0.36	0.34	0.32	0.29	0.27
13-year	0.45	0.45	0.44	0.43	0.41	0.39	0.37	0.34	0.32	0.29

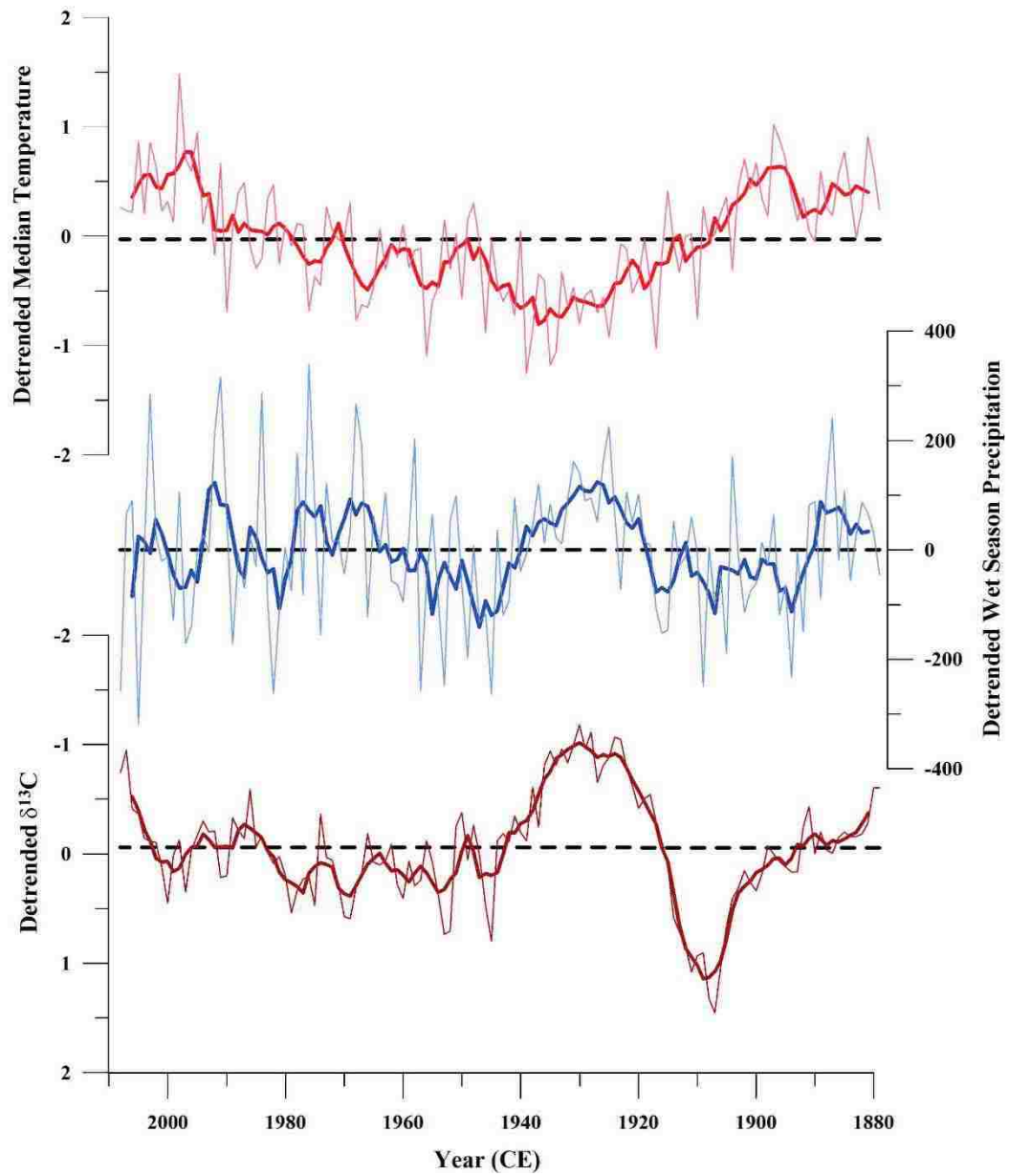


Figure 16 Detrended annual median temperature (red), detrended wet season rainfall totals (blue), and detrended yearly interpolated $\delta^{13}\text{C}$ values (brown) from JX-6 between 1880 to 2010 CE. Thick lines represent 5-year running averages and dashed lines represent linear trends (now detrended). Instrumental rainfall and temperature data collected from Tacubaya Station in Mexico City.

Table 5 Correlation coefficients for averaged $\delta^{13}\text{C}$ values to averaged $\delta^{18}\text{O}$ values, ^{24}Mg , $\log(^{24}\text{Mg})$, ^{238}U , and $\log(^{238}\text{U})$ from JX-6 using various running averages between 240 BCE to 2010 CE. Stable isotope values were averaged within trace element intervals to allow for correlations between different sampling resolutions. Bold values indicate the strongest correlations.

Average Resolution (years)	Running Average	Correlations to $\delta^{13}\text{C}$ (240 BCE – 2010 CE)				
		$\delta^{18}\text{O}$ (avg.)	^{24}Mg	$\log(^{24}\text{Mg})$	^{238}U	$\log(^{238}\text{U})$
4.26	Original Data	0.45	0.15	0.15	-0.29	-0.40
8.53	3-pt	0.46	0.25	0.22	-0.29	-0.41
17.07	5-pt	0.48	0.35	0.28	-0.28	-0.41
25.63	7-pt	0.49	0.40	0.32	-0.28	-0.40
34.22	9-pt	0.51	0.43	0.35	-0.27	-0.40
42.83	11-pt	0.52	0.45	0.36	-0.27	-0.39

Table 6 Correlation coefficients for averaged $\delta^{13}\text{C}$ values to averaged $\delta^{18}\text{O}$ values, ^{24}Mg , $\log(^{24}\text{Mg})$, ^{238}U , and $\log(^{238}\text{U})$ from JX-6 using various running averages between 240 BCE to 1800 CE. Stable isotope values were averaged within trace element intervals to allow for correlations between different sampling resolutions. Bold values indicate the strongest correlations. Original data and 11-point running averages plotted in Figure 17.

Average Resolution (years)	Running Average	Correlations to $\delta^{13}\text{C}$ (240 BCE – 1800 CE)				
		$\delta^{18}\text{O}$ (avg.)	^{24}Mg	$\log(^{24}\text{Mg})$	^{238}U	$\log(^{238}\text{U})$
4.26	Original Data	0.54	0.18	0.10	-0.36	-0.37
8.53	3-pt	0.54	0.29	0.17	-0.39	-0.41
17.07	5-pt	0.55	0.37	0.23	-0.39	-0.41
25.63	7-pt	0.57	0.42	0.27	-0.38	-0.40
34.22	9-pt	0.57	0.44	0.29	-0.38	-0.40
42.83	11-pt	0.58	0.45	0.31	-0.37	-0.40

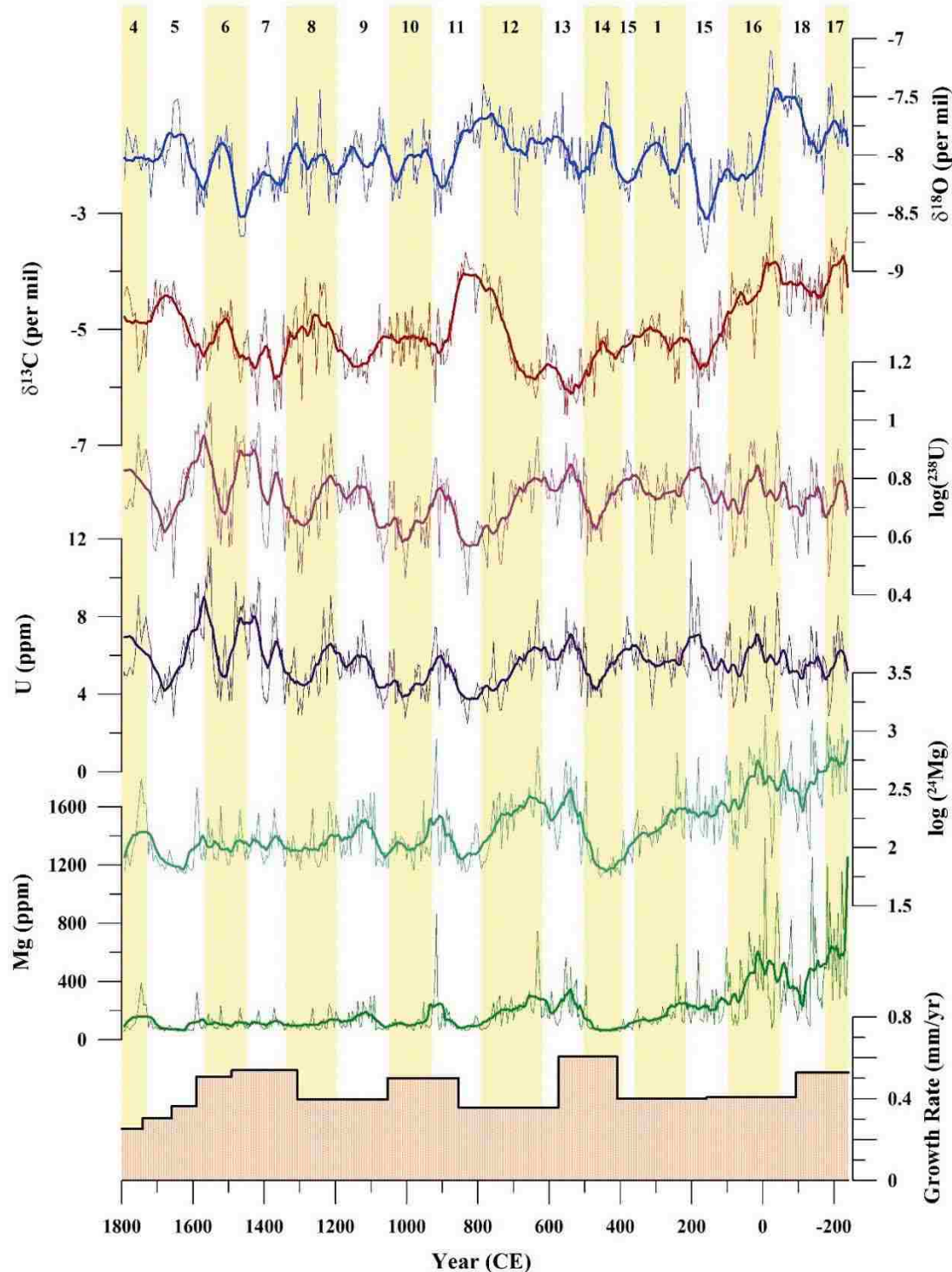


Figure 17 Graph showing the relationships between $\delta^{18}\text{O}$ (blue), $\delta^{13}\text{C}$ (red), $\log(^{238}\text{U})$ (light purple), U (dark purple), $\log(^{24}\text{Mg})$ (light green), and Mg (green) concentrations, and the growth rate (bottom) of JX-6 between 240 BCE to 1800 CE. Thick lines represent 11-point running averages. Numbers (top) and alternating white and yellow vertical bars correspond to different runs on the ICP-MS. Due to large trace element spikes, data between 1800 to 2010 CE was not plotted in this graph in order to show finer scale variability within the trace element concentrations across the majority of the time series. Uncertainty bars (1σ) plotted as black lines over trace element data are generally indistinguishable at this scale.

4.2 Uranium

U concentrations primarily vary between 3 – 10 ppm (Figure 18). However, there are a few distinct peaks around 1865, 1907, and 1935 CE of 23, 40, and 29 ppm, respectively. Due to these anomalous spikes in concentration relative to the preceding two millennia, it is suspected that these spikes in [U] were caused by non-climatic processes, and therefore were not correlated to instrumental rainfall and temperature data. Stable isotope values were averaged across trace element sampling intervals to permit correlations between different sampling resolutions. U exhibits a weak negative correlation to $\delta^{13}\text{C}$ ($r = -0.29$) across the 2,250 year time series (Table 7). This correlation improves ($r = -0.41$) if the $\log(^{238}\text{U})$ and 3-point running averages are used (Table 8). U also exhibits a weak positive correlation to ^{24}Mg and ^{25}Mg ($r = 0.31$) (Table 7). Removing the anomalous spikes in trace element concentrations post-1800 CE considerably increase the correlations between $\delta^{18}\text{O}$ and [U] ($r = -0.35$) and between $\delta^{18}\text{O}$ and $\log(^{238}\text{U})$ ($r = -0.36$) with no running averages are applied (Tables 9 and 10). Removing these most recent anomalous spikes (1800 – 2010 CE) also increases the correlation between [U] and $\delta^{13}\text{C}$ ($r = -0.36$) and between [U] and $\log(^{24}\text{Mg})$ ($r = 0.37$) (Table 9; Figure 17). All correlations involving [U] and the $\log(^{238}\text{U})$ with p -values > 0.05 are considered insignificant (Tables A7 – A10). Average relative standard deviation of ^{238}U for 500, 200, 100, 50, 20, and 5 ppb standard solutions are all ~2.5%, 1.1%, 1.0%, 0.8%, 0.9%, and 1.0%, respectively.

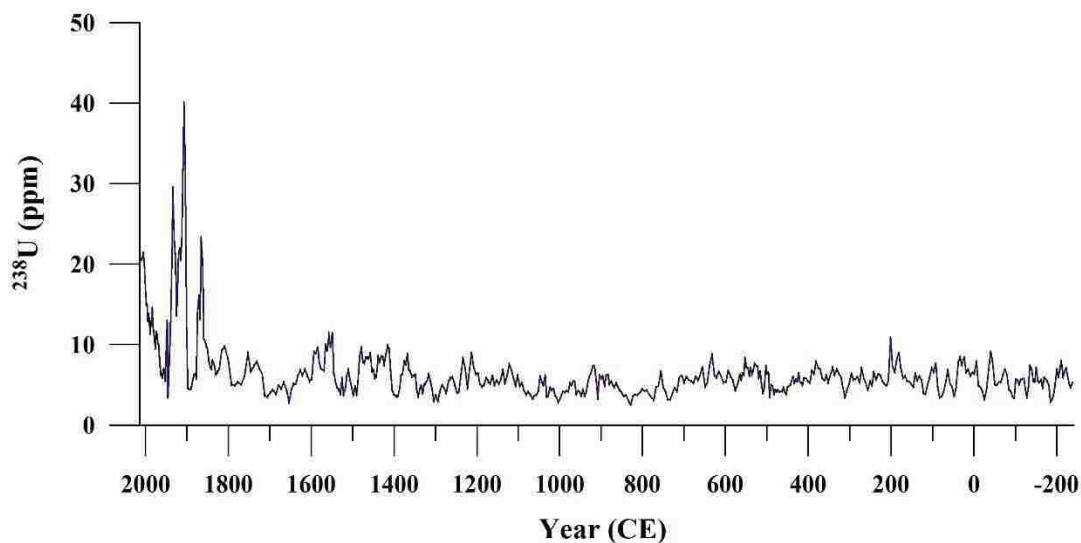


Figure 18 Uranium concentrations (ppm) of JX-6 between 240 BCE to 2010 CE. Uncertainty bars (1σ) plotted as black lines over [U] data are generally indistinguishable at this scale.

Table 7 Correlation coefficients for ^{238}U to averaged $\delta^{18}\text{O}$ and $\delta^{13}\text{C}$ values, ^{24}Mg , and $\log(^{24}\text{Mg})$ from JX-6 using various running averages between 240 BCE to 2010 CE. Stable isotope values were averaged within trace element intervals to allow for correlations between different sampling resolutions. Bold values indicate the strongest correlations. Original data and 11-point running averages plotted in Figure 17.

Average Resolution (years)	Running Average	Correlations to ^{238}U (240 BCE – 2010 CE)			
		$\delta^{18}\text{O}$ (avg.)	$\delta^{13}\text{C}$ (avg.)	^{24}Mg	$\log(^{24}\text{Mg})$
4.26	Original Data	-0.03	-0.29	0.31	0.15
8.53	3-pt	-0.01	-0.29	0.27	0.09
17.07	5-pt	0.00	-0.28	0.20	0.02
25.63	7-pt	0.01	-0.28	0.15	-0.04
34.22	9-pt	0.02	-0.27	0.11	-0.08
42.83	11-pt	0.03	-0.27	0.09	-0.12

Table 8 Correlation coefficients for the $\log(^{238}\text{U})$ to averaged $\delta^{18}\text{O}$ and $\delta^{13}\text{C}$ values, ^{24}Mg , and $\log(^{24}\text{Mg})$ from JX-6 using various running averages between 240 BCE to 2010 CE. Stable isotope values were averaged within trace element intervals to allow for correlations between different sampling resolutions. Bold values indicate the strongest correlations.

Average Resolution (years)	Running Average	Correlations to $\log(^{238}\text{U})$ (240 BCE – 2010 CE)			
		$\delta^{18}\text{O}$ (avg.)	$\delta^{13}\text{C}$ (avg.)	^{24}Mg	$\log(^{24}\text{Mg})$
4.26	Original Data	-0.14	-0.40	0.26	0.17
8.53	3-pt	-0.14	-0.41	0.22	0.10
17.07	5-pt	-0.13	-0.41	0.15	0.03
25.63	7-pt	-0.12	-0.40	0.11	-0.03
34.22	9-pt	-0.11	-0.40	0.08	-0.07
42.83	11-pt	-0.10	-0.39	0.06	-0.10

Table 9 Correlation coefficients for ^{238}U to averaged $\delta^{18}\text{O}$ and $\delta^{13}\text{C}$ values, ^{24}Mg , and $\log(^{24}\text{Mg})$ from JX-6 using various running averages between 240 BCE to 1800 CE. Stable isotope values were averaged within trace element intervals to allow for correlations between different sampling resolutions. Bold values indicate the strongest correlations. Original data and 11-point running averages plotted in Figure 17.

Average Resolution (years)	Running Average	Correlations to ^{238}U (240 BCE – 1800 CE)			
		$\delta^{18}\text{O}$ (avg.)	$\delta^{13}\text{C}$ (avg.)	^{24}Mg	$\log(^{24}\text{Mg})$
4.26	Original Data	-0.35	-0.36	0.30	0.37
8.53	3-pt	-0.39	-0.39	0.25	0.33
17.07	5-pt	-0.41	-0.39	0.21	0.28
25.63	7-pt	-0.43	-0.38	0.17	0.25
34.22	9-pt	-0.44	-0.38	0.16	0.23
42.83	11-pt	-0.45	-0.37	0.15	0.21

Table 10 Correlation coefficients for $\log(^{238}\text{U})$ to averaged $\delta^{18}\text{O}$ and $\delta^{13}\text{C}$ values, ^{24}Mg , and $\log(^{24}\text{Mg})$ from JX-6 using various running averages between 240 BCE to 1800 CE. Stable isotope values were averaged within trace element intervals to allow for correlations between different sampling resolutions. Bold values indicate the strongest correlations. Original data and 11-point running averages plotted in Figure 17.

Average Resolution (years)	Running Average	Correlations to $\log(^{238}\text{U})$ (240 BCE – 1800 CE)			
		$\delta^{18}\text{O}$ (avg.)	$\delta^{13}\text{C}$ (avg.)	^{24}Mg	$\log(^{24}\text{Mg})$
4.26	Original Data	-0.36	-0.37	0.31	0.38
8.53	3-pt	-0.40	-0.41	0.27	0.35
17.07	5-pt	-0.42	-0.41	0.22	0.31
25.63	7-pt	-0.43	-0.40	0.20	0.28
34.22	9-pt	-0.44	-0.40	0.19	0.26
42.83	11-pt	-0.44	-0.40	0.18	0.24

4.3 Magnesium, Strontium, and Barium

^{24}Mg and ^{25}Mg concentrations correlate very well ($r = 0.99$), and are separated by a maximum value of only 21 ppm across the 2,250 year time series. As a result, only ^{24}Mg concentrations are shown in figures and tables. Mg concentrations are characterized by many spikes overlying baseline values of ~80 ppm (Figure 19). Spikes are anywhere from 250 ppm to over 2,000 ppm, usually lasting 10 – 25 years (1 – 4 data points), with a maximum value of 2083 ppm around 1907 (Figure 19). Average relative standard deviation of ^{24}Mg for 500, 200, 100, 50, 20, and 5 ppb standard solutions are ~2.1%, 1.2%, 0.9%, 0.9%, 1.0%, and 1.0%, respectively. Average relative standard deviation of ^{25}Mg for 500, 200, 100, 50, 20, and 5 ppb standard solutions are ~2.2%, 1.4%, 0.8%, 1.2%, 1.5%, and 2.2%, respectively.

Strong shifts in [Sr] and [Ba] were observed between multiple runs. Because of the possibility of run-effects creating artificial relationships, [Sr] and [Ba] were not used in long term correlations. Despite the run effects, both Sr and Ba both reach maximum concentrations around 1904, of ~864 ppm and ~160 ppm, respectively. These maximum values are characterized by a large spike in concentration in the middle of Run 3, similar in time and magnitude to the spikes observed in [U] and [Mg]. These spikes are not associated with shifts in the drip axis or changes in the growth rate of JX-6 (Figure 20).

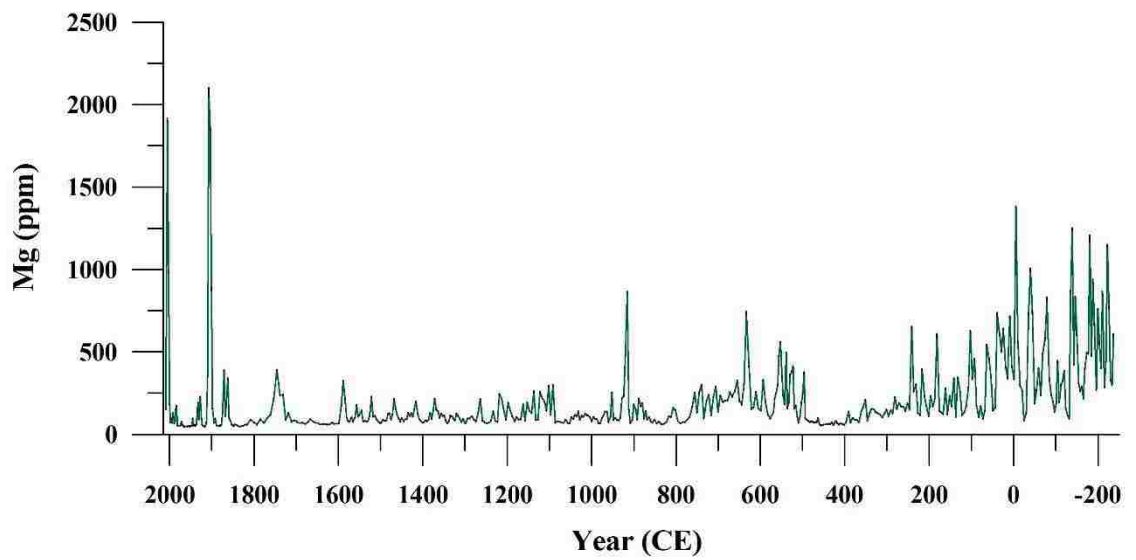


Figure 19 Magnesium (^{24}Mg) concentrations (ppm) of JX-6 between 240 BCE to 2010 CE. Uncertainty bars (1σ) plotted as black lines over [Mg] data are generally indistinguishable at this scale.

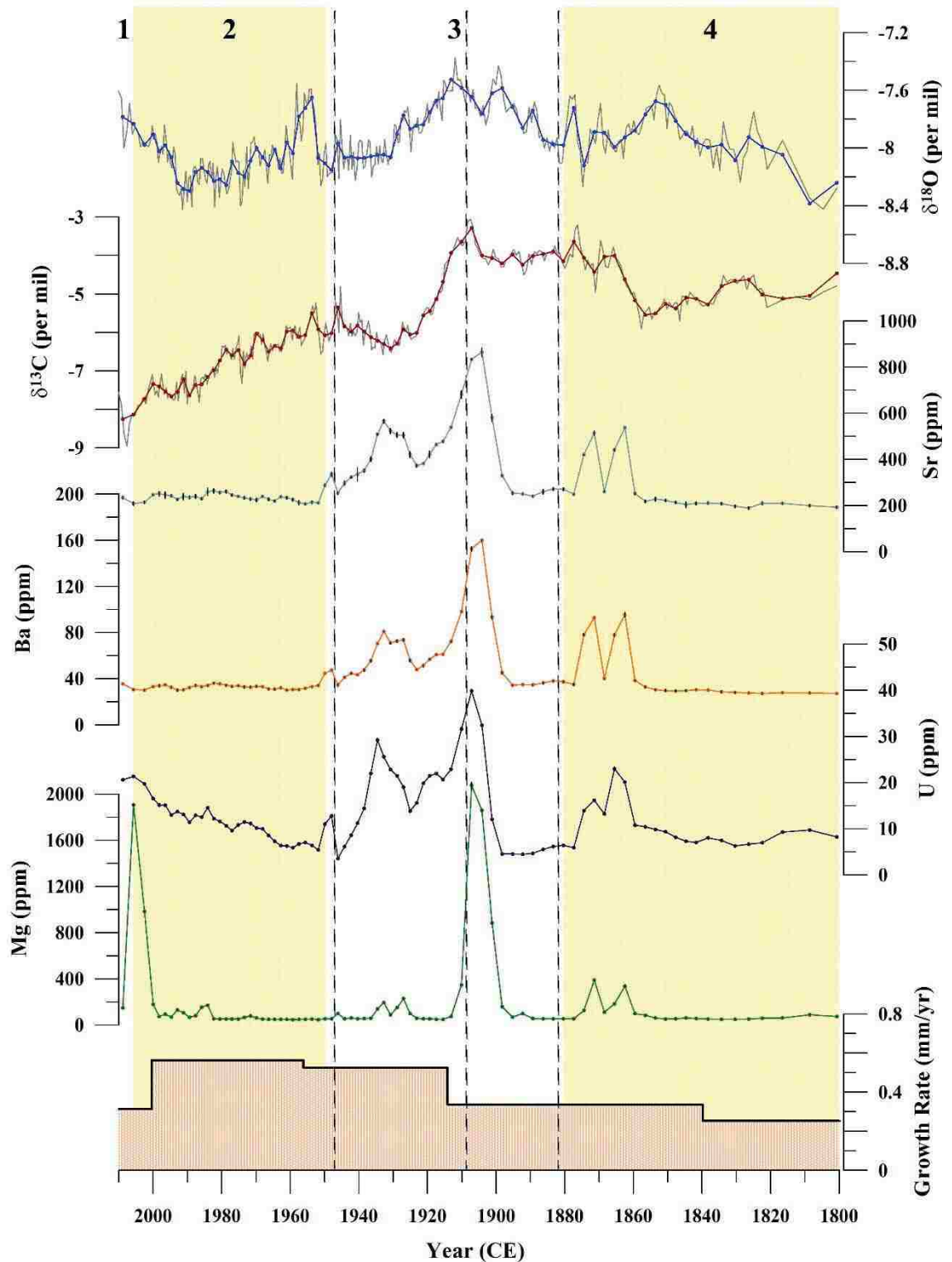


Figure 20 Graphs showing anomalous spikes in ^{84}Sr (gray), Ba (orange), U (purple), and ^{24}Mg (green) concentrations of JX-6 around 1862, 1871, 1904, and 1933 CE. These anomalous spikes are not observed in averaged $\delta^{18}\text{O}$ (blue) or averaged $\delta^{13}\text{C}$ (red) values (original $\delta^{18}\text{O}$ and $\delta^{13}\text{C}$ data shown in gray). Growth rate of JX-6 is shown on the bottom. Dashed vertical lines indicate a shift in the drip axis of JX-6. Numbers (top) and alternating yellow and white bars indicate different runs on the ICP-MS. Data plotted between 1800 to 2010 CE. Uncertainty bars (1σ) plotted as black lines over trace element data are generally indistinguishable at this scale.

5. Interpretations

5.1 Trace Element Anomalies

Trace element concentrations in JX-6 exhibit anomalous spikes in magnitude around 1862, 1871, 1904, and 1933 CE (Figure 21). The magnitude of these trace element variations significantly exceeds variability (more than 4 standard deviations) over the rest of the 2,250 year record. This indicates a large shift in the trace element concentrations in the dripwaters reaching stalagmite JX-6. Due to the magnitude of these spikes compared to the rest of the time series, they are interpreted to be related to anthropogenic impacts, possibly via deforestation above the cave. There is currently a small section of land cleared for agricultural or pastoral use above sections of Juxtlahuaca Cave (Figure 2). The initial clearing may have occurred in multiple events around 1862 to 1871 CE with a major clearing around 1904 CE. Agricultural use and tilling of the land may mobilize greater amounts of trace elements in the soil and allow greater amounts of rainfall to infiltrate into the epikarst. These combined processes may flush more trace elements, dissolved in the groundwater, into the cave and cause the anomalous spikes in concentrations observed in JX-6. The most significant of these spikes (~1904 – 1907 CE) corresponds to a slightly darker and denser growth layer (Figure 11). Due to no obvious color changes in JX-6 around 1862, 1871, and 1933 (Figure 11), it is likely that these spikes are not related to increased organic matter or soil particles being incorporated into the speleothem. Instead, I interpret the color change ~1904 to be related to changes in the density of aragonite at this specific growth layer.

Borsato et al. (2007) observed similar anomalous spikes in trace element concentrations in a stalagmite from Ernesto Cave, in northeast Italy, which were interpreted to be the result of a large deforestation event above the cave in association with pre-World War I operations. Their interpretation is supported by the timing of the spikes and historical archives. Unfortunately, no such records exist to my knowledge for the area above Juxtlahuaca Cave. However, based on their

association with darker growth layers and the magnitude of the spikes, it is probable that the cause of the large anomalies is anthropogenic. It is unlikely that these spikes are a climatic signal as there is no strong shift in rainfall amount or temperature in the instrumental record at this time (Figure 15).

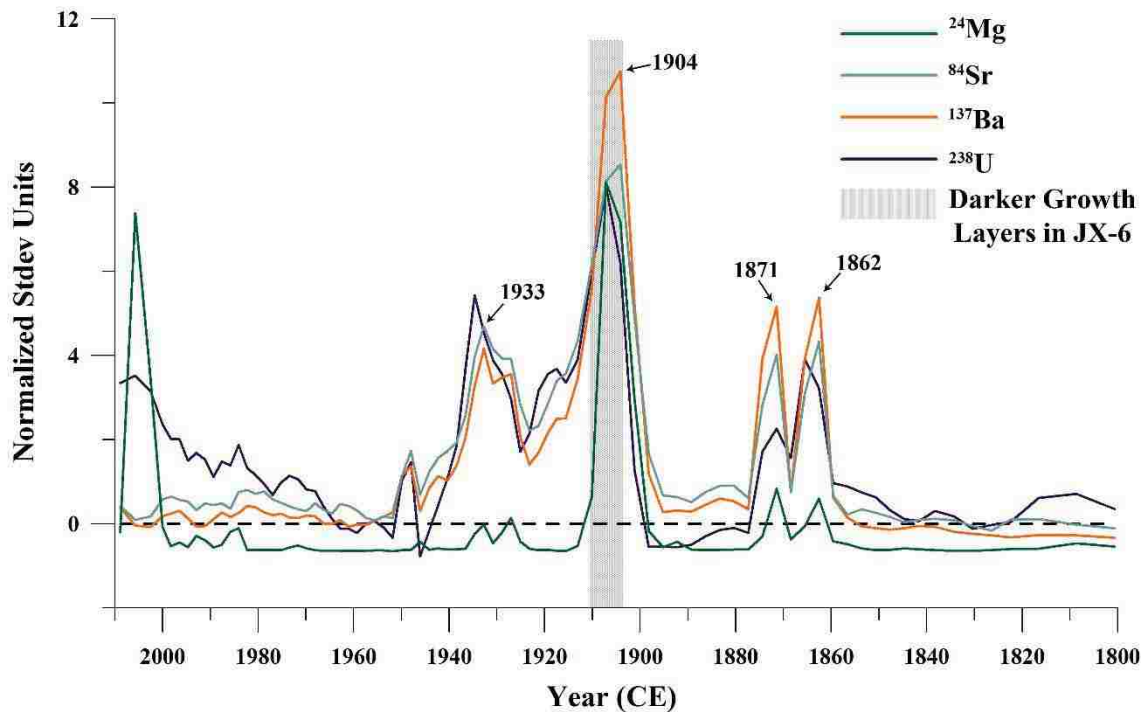


Figure 21 Graph showing normalized trace element concentrations in standard deviation units between 1800 to 2010 CE. ^{24}Mg (green), ^{84}Sr (gray), ^{137}Ba (orange), and ^{238}U (purple), all exhibit anomalous spikes around 1862, 1871, 1904, and 1933 CE. The most significant of these spikes ~1904 corresponds to darker growth layer within JX-6 (vertical gray bar).

5.2 Mechanisms Controlling $\delta^{13}\text{C}$ Values and $[U]$ in JX-6

The expected range of $\delta^{13}\text{C}$ values in an aragonitic speleothem precipitated in equilibrium conditions, with 90% of its carbon sourced from C3 type vegetation (-26‰ to -20‰) (McDermott, 2004) and the remaining 10% from carbonate bedrock (assumed to be ~0.35‰), should be -8.7‰ to -3.3‰. This range was calculated by first using the aragonite- CO_2 enrichment factor equation from Romanek et al. (1992):

$$\epsilon_{\text{ar-CO}_2} = 13.88 - 0.13 \cdot T (^{\circ}\text{C})$$

Where $\epsilon_{\text{ar-CO}_2}$ is the aragonite- CO_2 enrichment factor and T is temperature in degrees Celsius. This equation was used to account for the fractionation that occurs during the degassing process and precipitation of aragonite from cave dripwaters (+10.68‰ at 24.6°C) (Romanek et al, 1992). Fractionations that occur in the soil, due to preferential loss of ^{12}C to the atmosphere (+4.4‰), were also accounted for when calculating this range (Cerling & Quade, 1993). Determining the end members of this range results in the following equations:

$$(-26\text{‰} + 4.4\text{‰}) \cdot 0.9 + 0.35\text{‰} (0.1) + 10.68\text{‰} = \mathbf{-8.7\text{‰}} \quad (\text{low end})$$

$$(-20\text{‰} + 4.4\text{‰}) \cdot 0.9 + 0.35\text{‰} (0.1) + 10.68\text{‰} = \mathbf{-3.3\text{‰}} \quad (\text{high end})$$

In these equations, -26‰ and -20‰ are the expected low and high end ranges for $\delta^{13}\text{C}$ values sourced from C3-type vegetation (McDermott, 2004). The +4.4‰ accounts for the fractionation that occurs in the soil (Cerling & Quade, 1993). The 0.9 is assuming 90% of the carbon is sourced from the soil, the other 10% (0.1) is assumed to be sourced from the bedrock with a $\delta^{13}\text{C}$ value of +0.35‰. The +10.68‰ is the aragonite- CO_2 enrichment factor at 24.6°C (Romanek et al, 1992). Almost all of the $\delta^{13}\text{C}$ values (~99%) of JX-6 fall within the expected range of -8.7 to -3.3‰ (Figure 14), suggesting that it was precipitated at or near carbon isotopic equilibrium.

Cave temperatures are assumed to be consistent with mean annual surface temperatures ($\sim 24.6^{\circ}\text{C}$), and should not have significantly affected the $\delta^{13}\text{C}$ values of JX-6 over the last 2,250 years. Temperatures inside Juxtlahuaca would have had to vary by greater than 40°C to account for the range of $\delta^{13}\text{C}$ ($>5\text{‰}$) measured in JX-6. Due to the time scale involved, $\sim 2,250$ years, it is also unlikely that changes in the vegetation type (C3 vs C4) above Juxtlahuaca are responsible for these variations (Becerra, 2005).

Prior to detrending the data, all correlations between $\delta^{13}\text{C}$ and wet season rainfall are stronger than $r = -0.60$ (Table 1). The strongest correlation between detrended $\delta^{13}\text{C}$ and wet season rainfall ($r = -0.65$) occurs when no lag is applied to $\delta^{13}\text{C}$ and a 13-year running average is used for both $\delta^{13}\text{C}$ and wet season rainfall (Table 3). This strong correlation ($r = -0.65$) suggests that rainfall amount is a partial driver of the variations observed in the $\delta^{13}\text{C}$ values of JX-6. The negative correlation implies that $\delta^{13}\text{C}$ values will be more negative during years with increased amounts of wet season rainfall.

$\delta^{13}\text{C}$ also exhibits a negative correlation to $[\text{U}]$ ($r = -0.29$) (Table 5). This correlation coefficient increases when using the $\log(^{238}\text{U})$ and 3-point running averages ($r = -0.41$) (Table 8). The negative correlation demonstrates that during times of increasing $[\text{U}]$, $\delta^{13}\text{C}$ values are more negative. These correlations suggest that $\delta^{13}\text{C}$ and $[\text{U}]$ may be controlled by similar mechanisms. If this is the case, then $[\text{U}]$ should increase during periods of increased wet season rainfall. This interpretation is also supported by the negative correlation between $[\text{U}]$ and $\delta^{18}\text{O}$ values of JX-6 ($r = -0.35$) between 240 BCE to 1800 CE. Lachniet et al. (2012a) interpreted the $\delta^{18}\text{O}$ values as a proxy for rainfall amount over the last 2,250 years, suggesting more negative $\delta^{18}\text{O}$ values indicate greater amounts of rainfall (Figure 13). The negative correlation suggests that more negative $\delta^{18}\text{O}$ values, and therefore greater amounts of wet season rainfall, are associated with increased $[\text{U}]$ in JX-6. Due to the interpreted anthropogenic cause of the anomalous spikes in trace element concentrations after 1850 CE (Figure

20), correlations between [U] and wet season rainfall are considered invalid and are not reported in this study.

Given that JX-6 was likely precipitated in or near isotopic equilibrium and variations in the $\delta^{13}\text{C}$ values cannot be explained by changes in cave temperatures or shifts in vegetation type (C3 to C4), it is probable that the processes driving these variations occur in the soil and/or bedrock. The pH value of surface waters above Juxtlahuaca Cave are not known, and are not considered in this study. The area above the cave lies on a slope covered by a thin layer of soil, ~20 cm thick, sourced from the carbonate bedrock. As a result, it is unlikely that reducing conditions would occur, and therefore it is assumed that the soils above Juxtlahuaca are continually oxidized.

The strong correlations between $\delta^{13}\text{C}$, $\delta^{18}\text{O}$, and [U], discussed above, suggest that the variations observed in all three are partially driven by a similar mechanism related to wet season rainfall. Variations in the $p\text{CO}_2$ of overlying soils, due to changes in plant respiration, have been previously suggested as a driver of $\delta^{13}\text{C}$ in speleothems (Cruz et al., 2006; Linge et al., 2001) and may also affect [U] and mobility in groundwater (Langmuir, 1978).

Increased rainfall during the wet season should lead to an increase in the $p\text{CO}_2$ of the soil due to increased plant respiration, causing a decrease the $\delta^{13}\text{C}$ values of the soil (Fairchild et al., 2006; Cruz et al., 2006; Genty et al., 2001; Linge et al., 2001). This mechanism may explain the negative correlation observed between $\delta^{13}\text{C}$ and wet season rainfall. Changes in the $p\text{CO}_2$ of soils caused by increased plant respiration related to changes in wet season rainfall, may also affect the [U] in groundwater. U is commonly transported in groundwater in its hexavalent state [U(VI)] as the uranyl ion (UO_2^{2+}) (Langmuir, 1978; Sturchio et al., 1998). The mobility of UO_2^{2+} has been shown to increase with increasing $p\text{CO}_2$ (Langmuir, 1978). Therefore, increased $p\text{CO}_2$ in soils, via increased plant respiration during wetter periods, may lead to an increase in U being transported from soils to the cave. This mechanism would explain the negative correlation between $\delta^{13}\text{C}$ and [U] in JX-6 and suggests that [U] in speleothems may be a proxy for soil moisture. This

interpretation is supported by the positive correlation between $\delta^{13}\text{C}$ and $\delta^{18}\text{O}$, and the negative correlation between $\delta^{18}\text{O}$ and [U]. The $p\text{CO}_2$ mechanism is very similar to the processes involved in the phosphorus control hypothesis (Treble et al., 2003) mentioned in *Section 2.2*. This relationship is discussed further in *Section 6.1.3*.

6. Discussion

6.1 Comparison to Previous Speleothem [U] Studies

Comparing the interpretations of the mechanisms that control the [U] of JX-6 to previous studies in other locations may lead to a better understanding of the mechanisms that control [U] in speleothems:

1.) *Oxidation Control Hypothesis*: If the variations in [U] of JX-6 are controlled by increased biological activity in the soils, thus decreasing the oxidation of U to its more mobile state [U(VI)], then [U] would decrease during periods of greater biological activity (Hellstrom & McCulloch, 2000). For this study, it was assumed that increased biological activity in the soils above Juxtlahuaca Cave would occur during wetter growing seasons. Data from JX-6 suggests that [U] increases during periods of greater wet season rainfall (shown by lower $\delta^{13}\text{C}$ values). This is contradictory to what would be expected from Hellstrom & McCulloch's (2000) proposed mechanism. I infer that oxidation state in the soils is not a significant control on U mobility and dripwater [U] above Juxtlahuaca Cave. Therefore, this is most likely not the main driver of the variations in [U] observed in JX-6.

2.) *Prior Calcite Precipitation (PCP) Control Hypothesis*: If the variations in [U] of JX-6 are controlled by PCP due to U adsorbing onto mineral surfaces in the epikarst, then [U] would decrease in the stalagmite during drier periods and increase during wetter periods (Johnson et al., 2006). This hypothesis parallels my interpretation that increasing [U] in JX-6 indicate wetter periods. If PCP is a main driver of the variations in $\delta^{13}\text{C}$ and trace element concentrations in JX-6, I would also expect $\delta^{13}\text{C}$ and [Mg] to have a negative correlation to [U], as well as a positive correlation between $\delta^{13}\text{C}$ and [Mg]. This is due to the preferential loss of ^{12}C during the degassing process, enriching ground water in ^{13}C and therefore increasing the $\delta^{13}\text{C}$ of cave dripwaters during drier periods. This could explain the negative correlation between $\delta^{13}\text{C}$ and [U] observed in JX-6

Table 7). However, drier periods should also be indicated by increasing [Mg]. This is due to the preferential removal of Ca over Mg during the precipitation of calcite, enriching the groundwater in [Mg] during increased PCP. Instead, I observe that JX-6 [Mg] is positively correlated to [U] (Table 7), not negatively as found by Johnson et al. (2006), and only exhibit a large correlation to $\delta^{13}\text{C}$ values when large running averages are applied (Tables 5 and 6). $\delta^{13}\text{C}$ and [Mg] concentrations should also exhibit a positive correlation if prior aragonite precipitation (PAP) was occurring above Juxtlahuaca Cave, as opposed to PCP. This is due to the preferential degassing of ^{12}C over ^{13}C , and the preferential removal of Ca over Mg from groundwater during PAP. Therefore, it is likely that neither PCP nor PAP are the main driver of the variations in isotope and trace element concentrations observed in JX-6.

3.) *Phosphorus Control Hypothesis*: If the variations in [U] of JX-6 are controlled by the amount of P in the soil, [U] will increase during periods of higher vegetation decay, a major source of P in soils (Treble et al., 2003). P concentrations of JX-6 were not obtained during ICP-MS runs, and therefore cannot be directly correlated to [U]. However, Treble et al. (2003) suggest that increases in vegetation growth during the wet season may lead to overall increases in the amount of decaying vegetation. This suggests that wetter periods will lead to greater amounts of P in soils, and may explain the interpreted increase in [U] of JX-6 during wetter periods. Increased vegetation growth during wetter seasons should also lead to a decrease in the $\delta^{13}\text{C}$ of the soils due to increased plant respiration (discussed in *Section 5.2*), and therefore a decrease in the $\delta^{13}\text{C}$ in JX-6. This hypothesis is supported by the negative correlation between $\delta^{13}\text{C}$ and [U] in JX-6.

The processes controlling the amount of [P] in soils correspond to the same processes controlling the $p\text{CO}_2$ of the soil, the interpreted main driver of the variations in [U] of JX-6. It is possible that the [P] and the $p\text{CO}_2$ of soils are both controlling the [U] in JX-6. If this is the case, both should be increasing the mobility and concentrations of U in soils during periods of increased plant activity. Therefore, this still suggests that [U] in the groundwater may be directly affected by

the amount of plant activity in soils, and may be a suitable proxy for soil moisture when paired with $\delta^{13}\text{C}$ and $\delta^{18}\text{O}$ in speleothems.

6.2 Paleoclimate Implications

My interpretation that the [U] in JX-6 is a suitable proxy for soil moisture over the last 2,250 years, is largely based on the strong negative correlations between [U] and the stable isotopes $\delta^{18}\text{O}$ and $\delta^{13}\text{C}$ (Tables 7 – 10). I suggest that wetter periods, indicated by more negative $\delta^{18}\text{O}$ values (Lachniet et al., 2012a), would lead to increased plant respiration, increasing the $p\text{CO}_2$ of the soil. This would decrease the $\delta^{13}\text{C}$ values in the soil, and therefore decrease the $\delta^{13}\text{C}$ of dissolved inorganic carbon in the water transported from the soil to the cave (Cruz et al., 2006; Linge et al., 2001). This increased $p\text{CO}_2$ would also mobilize more U in the soil (Langmuir, 1978), eventually increasing the [U] in cave dripwaters. However, the amount of plant respiration occurring in a soil is not exclusively related to the total amount of rainfall that occurs within a given season. The regularity of rainfall within a season, as well as variations in temperature, must also have an effect on the amount of moisture a soil can store, and therefore should have an effect on the $p\text{CO}_2$ within the soil.

Assuming rainfall remains constant, increased evapotranspiration during periods of increased temperatures may decrease overall soil moisture. Depending on the magnitude of the temperature increase, this may lead to a decrease in plant respiration, and therefore a decrease in $p\text{CO}_2$ in the soils. I would expect the [U] to decrease and $\delta^{13}\text{C}$ to increase in cave dripwaters during this time, due to a decrease in $p\text{CO}_2$ of the soils. However, this temperature increase may not be displayed in the $\delta^{18}\text{O}$ signal of cave dripwaters if annual rainfall remains constant. A similar signal may result from an exceptionally dry season (decreased [U]) in which a few large storms with very depleted $\delta^{18}\text{O}$ values overwhelm the overall signal. In this scenario, a significant dry period may be misinterpreted as very wet when solely utilizing the $\delta^{18}\text{O}$ values. These examples demonstrate some

of the complexities that can arise when interpreting a single speleothem proxy data set. However, they also illustrate the benefits of having a multiproxy record in a single stalagmite.

Combining the signals from all three datasets ($\delta^{18}\text{O}$, $\delta^{13}\text{C}$, and [U]) may allow for a more accurate representation of how climate has varied in southwestern Mexico over the last 2,250 years (Figure 22). Using the mean values of each proxy to designate dry periods from wet periods, I found that over ~15% (80 out of 529 samples) of the time series (240 BCE – 2010 CE), all three proxies simultaneously indicate wet periods. Meaning that the $\delta^{13}\text{C}$ and $\delta^{18}\text{O}$ were below their respective mean values (more negative) at the same time that [U] were above their mean values. I would expect consistent wet season rainfall during these time intervals, in which temperatures are not too hot or too cold to inhibit plant growth. These wet periods are most evident between ~1400 – 1500 CE and ~1550 – 1600 CE. There are also a few short, intermittent wet periods between 100 – 550 CE (Figure 22).

I also found that over ~24% (127 out of 529 samples) of the time series (240 BCE – 2010 CE), all three proxies simultaneously indicate drier periods. This means that the $\delta^{13}\text{C}$ and $\delta^{18}\text{O}$ were above (more positive) their respective mean values at the same time that [U] were below their mean values. Though extreme temperature changes may result in decreased plant growth, I expect decreased rainfall to be the major cause of the overall drought signal during these time intervals. Several extended dry periods are evident in these data sets, including: ~240 – 50 BCE; ~700 – 850 CE; and ~1600 – 1700 CE. There are also numerous intermittent dry periods between ~200 – 500 CE and ~900 – 1350 CE (Figure 22).

Lachniet et al. (2012a) relate their 2,250 year rainfall reconstruction, based solely on the $\delta^{18}\text{O}$ values of JX-6, to key cultural changes in large Mesoamerican cities. Teotihuacan was one of the first of these major urban centers (100 BCE to 600 CE) in the Basin of Mexico. Lachniet et al. (2012a) suggest that the early settlement of Teotihuacan (200 BCE – 0 CE) occurred during a drier than average period. The $\delta^{13}\text{C}$ and [U] also indicate an extended drought at this time. Although the

7-point running average of [U] in Figure 22 suggests possible wet periods during this time, the overall signal is in agreement with a long-term drought (indicated by the vertical red lines in Figure 22). Lachniet et al. (2012a) also propose that the decline of Teotihuacan (~550 CE) occurred after a multi-century long drying trend (~100 to 600 CE), followed by a ~150 year long drought (Figure 22). The [U] and $\delta^{13}\text{C}$ values from JX-6 also show this same multi-century drying trend, followed by the same ~150 year drought (Figure 22). Lachniet et al. (2012a) interpret the sharp increase in $\delta^{18}\text{O}$ values ~900 CE as the end of this extended drought period. However, the decreased [U] continues to ~1100 CE, suggesting dry conditions lasted beyond the interval inferred from $\delta^{18}\text{O}$ values. This may indicate an overall dry period, dominated by large, infrequent storm rainfall, which may explain some of the more negative $\delta^{18}\text{O}$ values observed at this time (~900 – 1100 CE). My observation of a more extensive drought between 700 – 1100 CE supports the notion of an extended drought during the Terminal Classic Collapse (750-1050 CE), which has been associated with the collapse of the lowland Maya civilizations (Hodell et al., 2007).

The rainfall reconstruction from Lachniet et al. (2012a) is also interpreted as exhibiting a sharp increase in rainfall ~1450 CE, which they relate to periods of observed flooding and dike construction near the Aztec city of Tenochtitlan. The [U] and $\delta^{13}\text{C}$ values also indicate this rapid increase in rainfall around this time (Figure 22). Furthermore, all three data sets display a similar trend towards wetter conditions between ~1250 – 1450 CE, followed by a drying trend between ~1450 -1800 CE. Overall, my interpretations of the climatic conditions of southwestern Mexico over the last 2,250 years, based on the [U] and $\delta^{13}\text{C}$ of JX-6, agree with previous interpretations based solely on the $\delta^{18}\text{O}$ values (Lachniet et al., 2012a). However, these new data suggest extended dry conditions between ~925 – 1100 CE, as inferred by low [U] in the stalagmite, whereas the low $\delta^{18}\text{O}$ values may have been influenced by strong but infrequent large storms.

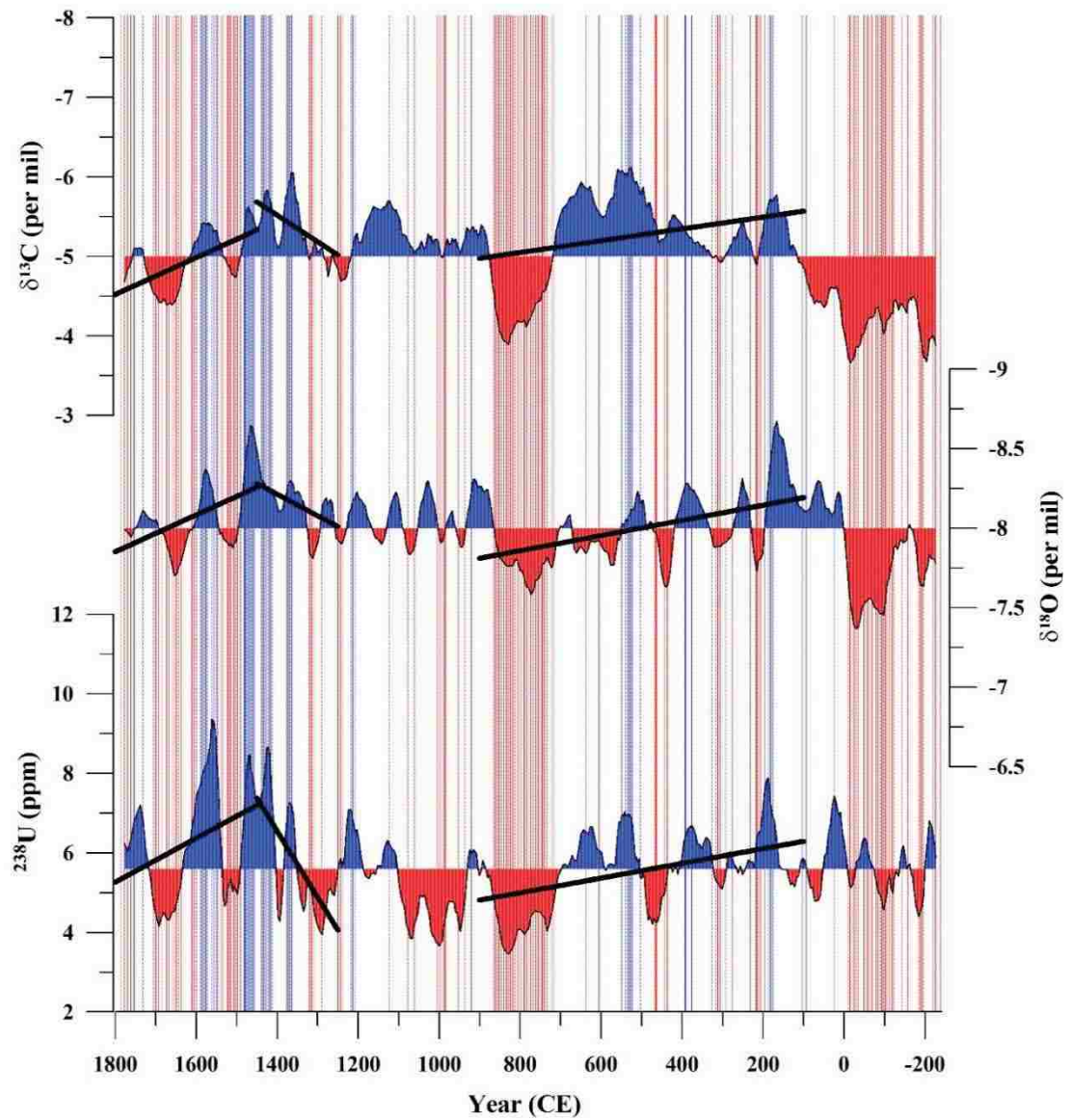


Figure 22 $\delta^{13}\text{C}$, $\delta^{18}\text{O}$, and $[\text{U}]$ 7-point running averages plotted from JX-6 between 240 BCE to 1800 CE shown shaded in blue (above the mean) and red (below the mean). Blue and red shading based on means calculated from original data between 240 BCE to 1800 BCE. Vertical light blue and light red bars indicate significant periods in which all three data sets are above (blue) and below (red) their respective mean values. Thick black lines indicate specific trends (100 – 900 CE; 1250 – 1450 CE; 1450 – 1800 CE) based on interpreted trends in the $\delta^{18}\text{O}$ from Lachniet et al. (2012a).

7. Conclusions

Trace element concentrations in speleothems can be useful proxies for paleoclimatic conditions and may be used as a signal of anthropogenic environmental changes occurring at the surface. JX-6 exhibits anomalous spikes in trace element concentrations around 1862, 1871, 1904, and 1933 CE. These spikes are interpreted as being related to deforestation events above Juxtlahuaca Cave in association with clearing of the land for agricultural use.

The variations in [U] of JX-6 are interpreted to be controlled by changes in the $p\text{CO}_2$ of overlying soils. This interpretation is based on the negative correlations between [U] and the stable isotopes $\delta^{13}\text{C}$ and $\delta^{18}\text{O}$. Assuming that $p\text{CO}_2$ will increase during periods of increased plant respiration, mobilizing greater amounts of U within the soil, [U] of JX-6 may be a proxy for soil moisture above Juxtlahuaca Cave. The interpretations from this study disagree with the oxidation control hypothesis of Hellstrom & McCulloch (2000) and with the PCP control hypothesis of Johnson et al. (2006). With current trace element data, this study is unable to directly test the phosphorus control hypothesis of Treble et al. (2003). However, the interpretations from this study relate very closely to the processes discussed in Treble et al. (2003), and the [U] of JX-6 may also be affected by [P] in the soil. However, if this is the case, a similar signal would be expected in the [U] of JX-6. Instead, I suggest that increased soil productivity, as inferred by low $\delta^{13}\text{C}$ values in JX-6, was associated with greater U leaching from soils during wet periods, and that this resulted in higher speleothem [U], consistent with the mechanisms detailed by Langmuir (1978).

Based on previous work (Hellstrom & McCulloch, 2000; Johnson et al., 2006; Treble et al., 2003) and the interpretations of this study, [U] in speleothems seem to be driven by local cave conditions. Therefore, [U] cannot be used as a reliable proxy for paleoclimatic conditions without the support of additional trace element and stable isotope data. U concentrations in speleothems can however assist in the complex interpretations of other speleothem proxies. To better understand the mechanisms controlling [U] in JX-6, future work in Juxtlahuaca should focus on measuring [P],

seasonal changes in $p\text{CO}_2$, and oxidation conditions in the soil overlying the cave. These data would help to better understand the mechanisms controlling [U] and their relationship to paleoclimate.

Appendix

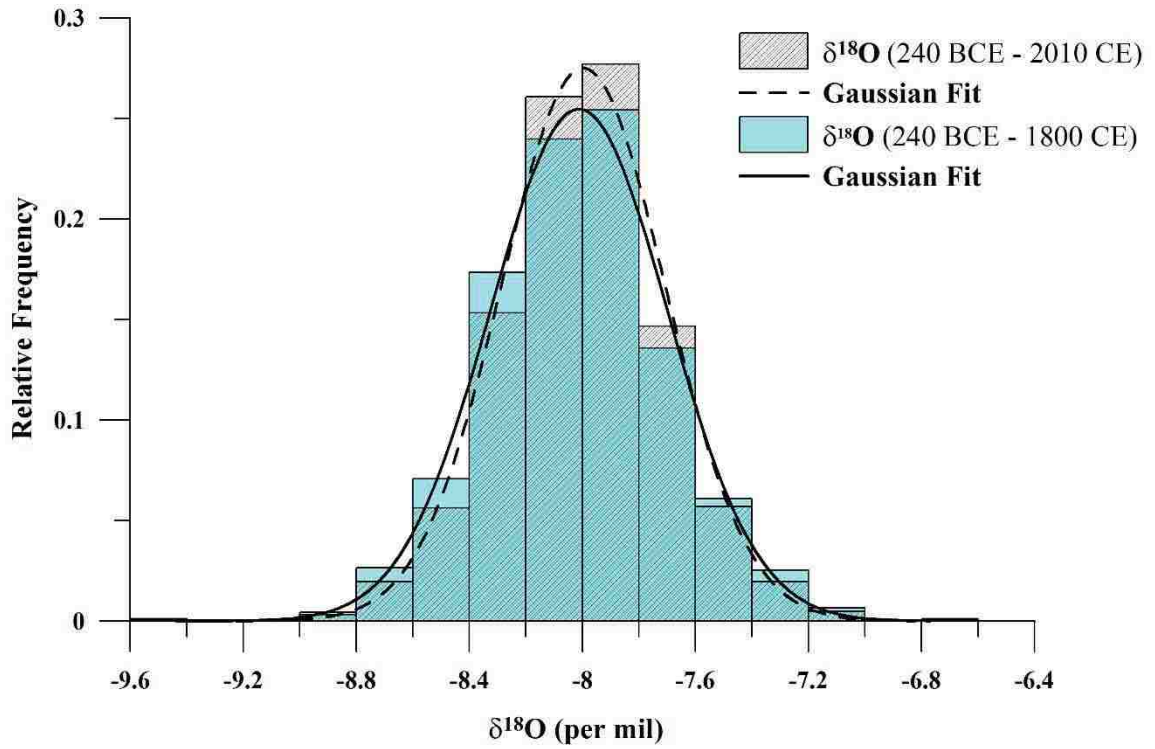


Figure A1 Histogram showing the relative frequency of $\delta^{18}\text{O}$ values of JX-6 between 240 BCE – 2010 CE (slashed bars and dashed line) and between 240 BCE – 1800 CE (light blue bars and solid line). Data separated to show difference in distribution between time periods with and without anomalous spikes in trace element concentrations (1800 – 2010 CE).

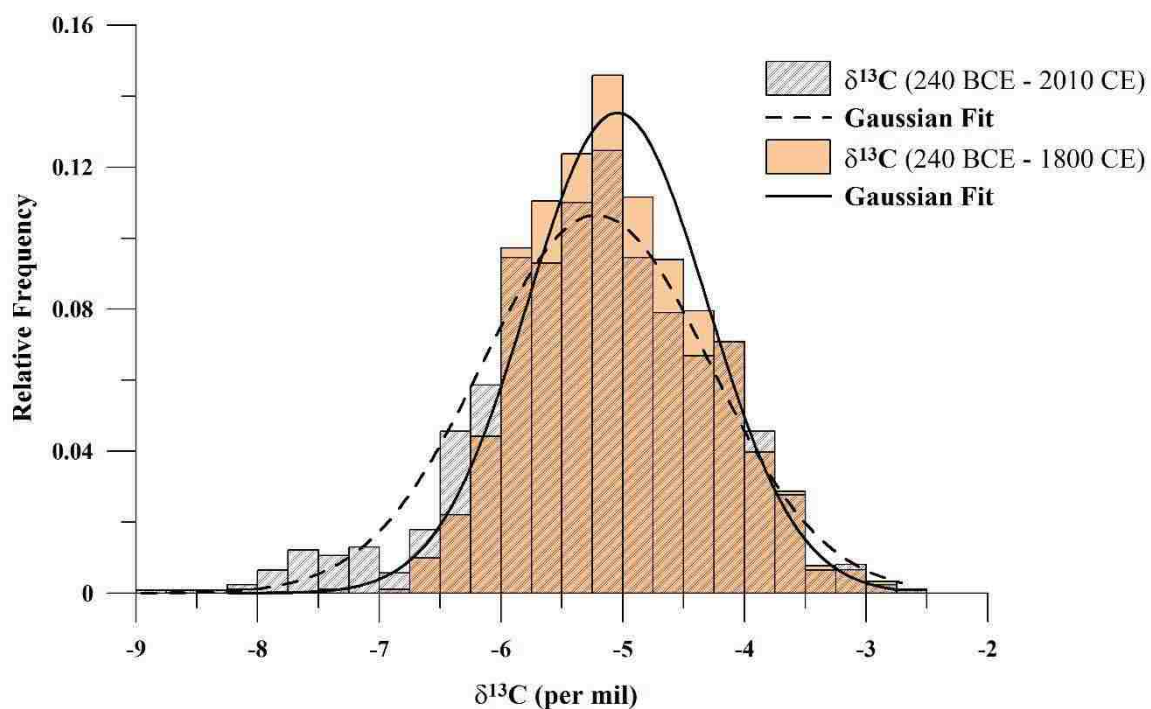


Figure A2 Histogram showing the relative frequency of $\delta^{13}\text{C}$ values of JX-6 between 240 BCE – 2010 CE (slashed bars and dashed line) and between 240 BCE – 1800 CE (light orange bars and solid line). Data separated to show difference in distribution between time periods with and without anomalous spikes in trace element concentrations (1800 – 2010 CE).

Table A1 Significance (p) values for correlations between yearly interpolated $\delta^{13}\text{C}$ of JX-6 and wet season rainfall (May – November) with various running averages and yearly lags in $\delta^{13}\text{C}$ values between 1880 to 2010 CE (see Table 1). Italic values indicate p -values > 0.05 .

p-Values for Correlations between $\delta^{13}\text{C}$ and Wet Season Rainfall (1880 – 2010 CE)										
Running Average	Lag in $\delta^{13}\text{C}$ (years)									
	No Lag	1	2	3	4	5	6	7	8	9
Original Data	0.000	0.000	0.000	0.000	0.000	0.000	0.000	0.000	0.000	0.000
3-year	0.000	0.000	0.000	0.000	0.000	0.000	0.000	0.000	0.000	0.000
5-year	0.000	0.000	0.000	0.000	0.000	0.000	0.000	0.000	0.000	0.000
7-year	0.000	0.000	0.000	0.000	0.000	0.000	0.000	0.000	0.000	0.000
9-year	0.000	0.000	0.000	0.000	0.000	0.000	0.000	0.000	0.000	0.000
11-year	0.000	0.000	0.000	0.000	0.000	0.000	0.000	0.000	0.000	0.000
13-year	0.000	0.000	0.000	0.000	0.000	0.000	0.000	0.000	0.000	0.000

Table A2 Significance (*p*) values for correlations between yearly interpolated $\delta^{13}\text{C}$ of JX-6 and median annual temperature with various running averages and yearly lags in $\delta^{13}\text{C}$ values between 1880 to 2010 CE (see Table 2). Italic values indicate *p*-values > 0.05.

<i>p</i>-Values for Correlations between $\delta^{13}\text{C}$ and Median Temperature (1880 – 2010 CE)										
Running Average	Lag in $\delta^{13}\text{C}$ (years)									
	No Lag	1	2	3	4	5	6	7	8	9
Original Data	0.000	0.000	0.000	0.000	0.000	0.000	0.000	0.000	0.000	0.000
3-year	0.000	0.000	0.000	0.000	0.000	0.000	0.000	0.000	0.000	0.000
5-year	0.000	0.000	0.000	0.000	0.000	0.000	0.000	0.000	0.000	0.000
7-year	0.000	0.000	0.000	0.000	0.000	0.000	0.000	0.000	0.000	0.000
9-year	0.000	0.000	0.000	0.000	0.000	0.000	0.000	0.000	0.000	0.000
11-year	0.000	0.000	0.000	0.000	0.000	0.000	0.000	0.000	0.000	0.000
13-year	0.000	0.000	0.000	0.000	0.000	0.000	0.000	0.000	0.000	0.000

Table A3 Significance (*p*) values for correlations between detrended yearly interpolated $\delta^{13}\text{C}$ of JX-6 and detrended wet season rainfall (May – November) with various running averages and yearly lags in $\delta^{13}\text{C}$ values between 1880 to 2010 CE (see Table 3). Italic values indicate *p*-values > 0.05.

<i>p</i>-Values for Correlations between Detrended $\delta^{13}\text{C}$ and Wet Season Rainfall (1880 – 2010 CE)										
Running Average	Lag in $\delta^{13}\text{C}$ (years)									
	No Lag	1	2	3	4	5	6	7	8	9
Original Data	0.012	0.010	0.001	0.039	0.007	0.033	<i>0.160</i>	<i>0.130</i>	0.033	<i>0.491</i>
3-year	0.000	0.000	0.000	0.000	0.000	0.000	0.001	0.008	0.037	<i>0.248</i>
5-year	0.000	0.000	0.000	0.000	0.000	0.000	0.000	0.002	0.023	<i>0.266</i>
7-year	0.000	0.000	0.000	0.000	0.000	0.000	0.000	0.000	0.017	<i>0.273</i>
9-year	0.000	0.000	0.000	0.000	0.000	0.000	0.000	0.000	0.020	<i>0.266</i>
11-year	0.000	0.000	0.000	0.000	0.000	0.000	0.000	0.001	0.023	<i>0.265</i>
13-year	0.000	0.000	0.000	0.000	0.000	0.000	0.000	0.001	0.028	<i>0.291</i>

Table A4 Significance (p) values for correlations between detrended yearly interpolated $\delta^{13}\text{C}$ of JX-6 and detrended annual median temperature with various running averages and yearly lags in $\delta^{13}\text{C}$ values between 1880 to 2010 CE (see Table 4). Italic values indicate p -values > 0.05 .

p-Values for Correlations between Detrended $\delta^{13}\text{C}$ and Median Temperature (1880 – 2010 CE)										
Running Average	Lag in $\delta^{13}\text{C}$ (years)									
	No Lag	1	2	3	4	5	6	7	8	9
Original Data	0.010	0.012	0.011	0.008	0.007	0.029	0.033	0.036	0.009	<i>0.219</i>
3-year	0.001	0.000	0.000	0.000	0.001	0.002	0.003	0.004	0.011	0.050
5-year	0.000	0.000	0.000	0.000	0.000	0.000	0.001	0.002	0.007	0.023
7-year	0.000	0.000	0.000	0.000	0.000	0.000	0.000	0.001	0.004	0.015
9-year	0.000	0.000	0.000	0.000	0.000	0.000	0.000	0.001	0.002	0.008
11-year	0.000	0.000	0.000	0.000	0.000	0.000	0.000	0.000	0.001	0.004
13-year	0.000	0.000	0.000	0.000	0.000	0.000	0.000	0.000	0.000	0.001

Table A5 Significance (p) values for correlations between averaged $\delta^{13}\text{C}$ to averaged $\delta^{18}\text{O}$, ^{24}Mg , $\log(^{24}\text{Mg})$, ^{238}U , and $\log(^{238}\text{U})$ from JX-6 using various running averages between 240 BCE to 2010 CE (see Table 5).

Average Resolution (years)	Running Average	p-Values for Correlations to $\delta^{13}\text{C}$ (240 BCE – 2010 CE)				
		$\delta^{18}\text{O}$ (avg.)	^{24}Mg	$\log(^{24}\text{Mg})$	^{238}U	$\log(^{238}\text{U})$
4.26	Original Data	0.000	0.001	0.001	0.000	0.000
8.53	3-pt	0.000	0.000	0.000	0.000	0.000
17.07	5-pt	0.000	0.000	0.000	0.000	0.000
25.63	7-pt	0.000	0.000	0.000	0.000	0.000
34.22	9-pt	0.000	0.000	0.000	0.000	0.000
42.83	11-pt	0.000	0.000	0.000	0.000	0.000

Table A6 Significance (p) values for correlations between averaged $\delta^{13}\text{C}$ to averaged $\delta^{18}\text{O}$, ^{24}Mg , $\log(^{24}\text{Mg})$, ^{238}U , and $\log(^{238}\text{U})$ from JX-6 using various running averages between 240 BCE to 2010 CE (see Table 6).

Average Resolution (years)	Running Average	<i>p</i>-Values for Correlations to $\delta^{13}\text{C}$ (240 BCE – 1800 CE)				
		$\delta^{18}\text{O}$ (avg.)	^{24}Mg	$\log(^{24}\text{Mg})$	^{238}U	$\log(^{238}\text{U})$
4.26	Original Data	0.000	0.000	0.041	0.000	0.000
8.53	3-pt	0.000	0.000	0.000	0.000	0.000
17.07	5-pt	0.000	0.000	0.000	0.000	0.000
25.63	7-pt	0.000	0.000	0.000	0.000	0.000
34.22	9-pt	0.000	0.000	0.000	0.000	0.000
42.83	11-pt	0.000	0.000	0.000	0.000	0.000

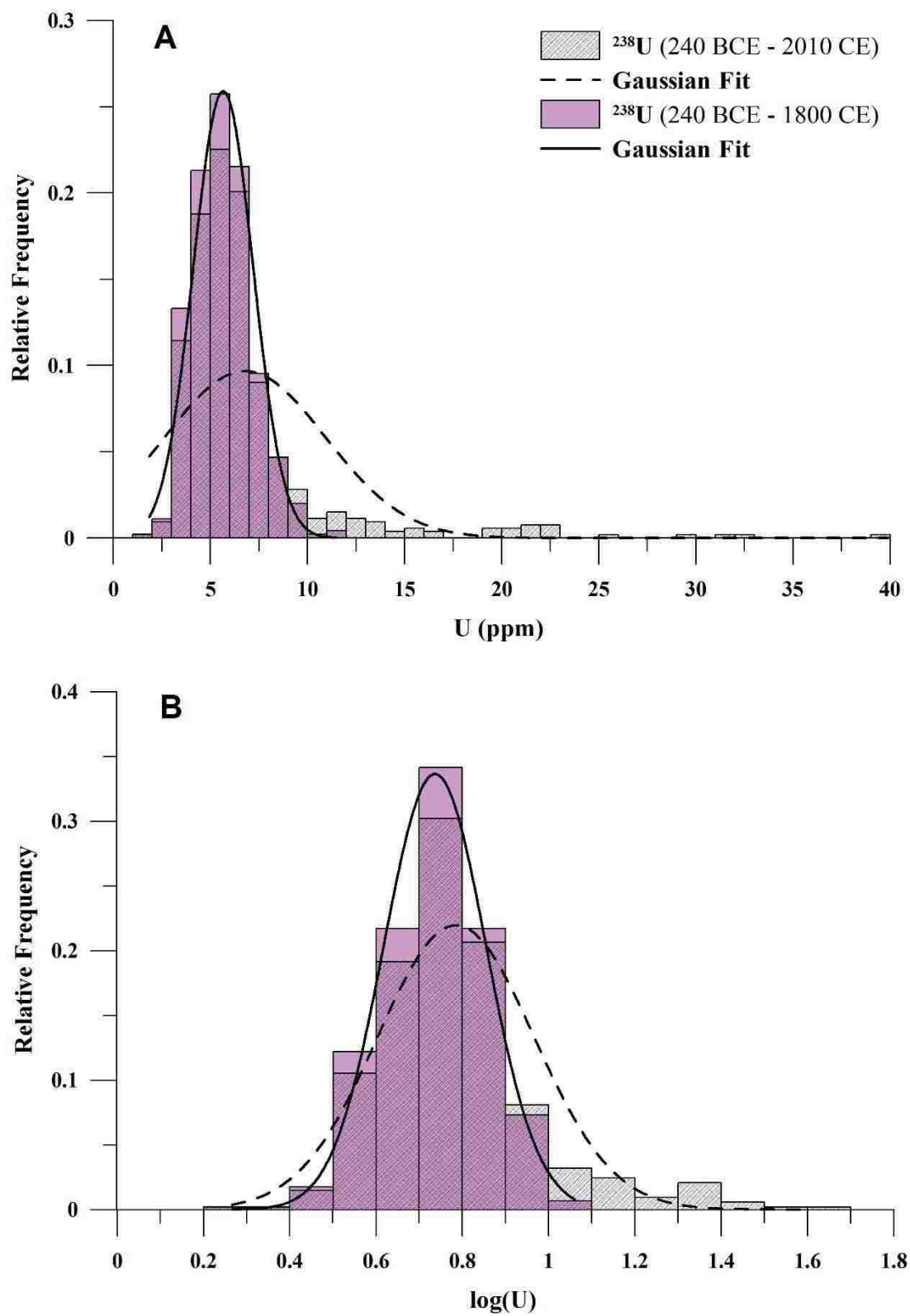


Figure A3 Histograms showing (A) [U] and (B) log(U) of JX-6 between 240 BCE – 2010 CE (slashed bars and dashed line) and between 240 BCE – 1800 CE (purple bars and solid line). Data separated to show difference in distribution between time periods with and without anomalous spikes in trace element concentrations (1800 – 2010 CE).

Table A7 Significance (p) values for correlations between ^{238}U to $\delta^{18}\text{O}$, $\delta^{13}\text{C}$, ^{24}Mg , and $\log(^{24}\text{Mg})$ from JX-6 using various running averages between 240 BCE to 2010 CE (see Table 7). Italic values indicate p -values > 0.05 .

Average Resolution (years)	Running Average	p-Values for Correlations to ^{238}U (240 BCE – 2010 CE)			
		$\delta^{18}\text{O}$ (avg.)	$\delta^{13}\text{C}$ (avg.)	^{24}Mg	$\log(^{24}\text{Mg})$
4.26	Original Data	<i>0.531</i>	0.000	0.000	0.000
8.53	3-pt	<i>0.773</i>	0.000	0.000	0.032
17.07	5-pt	<i>0.973</i>	0.000	0.000	<i>0.649</i>
25.63	7-pt	<i>0.781</i>	0.000	0.001	<i>0.387</i>
34.22	9-pt	<i>0.643</i>	0.000	0.009	<i>0.062</i>
42.83	11-pt	<i>0.478</i>	0.000	0.044	0.008

Table A8 Significance (p) values for correlations between $\log(^{238}\text{U})$ to $\delta^{18}\text{O}$, $\delta^{13}\text{C}$, ^{24}Mg , and $\log(^{24}\text{Mg})$ from JX-6 using various running averages between 240 BCE to 2010 CE (see Table 8). Bold and italic values indicate p -values > 0.05 .

Average Resolution (years)	Running Average	p-Values for Correlations to $\log(^{238}\text{U})$ (240 BCE – 2010 CE)			
		$\delta^{18}\text{O}$ (avg.)	$\delta^{13}\text{C}$ (avg.)	^{24}Mg	$\log(^{24}\text{Mg})$
4.26	Original Data	0.001	0.000	0.000	0.000
8.53	3-pt	0.001	0.000	0.000	0.019
17.07	5-pt	0.003	0.000	0.000	<i>0.523</i>
25.63	7-pt	0.007	0.000	0.012	<i>0.494</i>
34.22	9-pt	0.013	0.000	<i>0.062</i>	<i>0.104</i>
42.83	11-pt	0.027	0.000	<i>0.163</i>	0.019

Table A9 Significance (p) values for correlations between ^{238}U to $\delta^{18}\text{O}$, $\delta^{13}\text{C}$, ^{24}Mg , and $\log(^{24}\text{Mg})$ from JX-6 using various running averages between 240 BCE to 1800 CE (see Table 9).

Average Resolution (years)	Running Average	p-Values for Correlations to ^{238}U (240 BCE – 1800 CE)			
		$\delta^{18}\text{O}$ (avg.)	$\delta^{13}\text{C}$ (avg.)	^{24}Mg	$\log(^{24}\text{Mg})$
4.26	Original Data	0.000	0.000	0.000	0.000
8.53	3-pt	0.000	0.000	0.000	0.000
17.07	5-pt	0.000	0.000	0.000	0.000
25.63	7-pt	0.000	0.000	0.000	0.000
34.22	9-pt	0.000	0.000	0.001	0.000
42.83	11-pt	0.000	0.000	0.002	0.000

Table A10 Significance (p) values for correlations between $\log(^{238}\text{U})$ to $\delta^{18}\text{O}$, $\delta^{13}\text{C}$, ^{24}Mg , and $\log(^{24}\text{Mg})$ from JX-6 using various running averages between 240 BCE to 1800 CE (see Table 10).

Average Resolution (years)	Running Average	p-Values for Correlations to $\log(^{238}\text{U})$ (240 BCE – 1800 CE)			
		$\delta^{18}\text{O}$ (avg.)	$\delta^{13}\text{C}$ (avg.)	^{24}Mg	$\log(^{24}\text{Mg})$
4.26	Original Data	0.000	0.000	0.000	0.000
8.53	3-pt	0.000	0.000	0.000	0.000
17.07	5-pt	0.000	0.000	0.000	0.000
25.63	7-pt	0.000	0.000	0.000	0.000
34.22	9-pt	0.000	0.000	0.000	0.000
42.83	11-pt	0.000	0.000	0.000	0.000

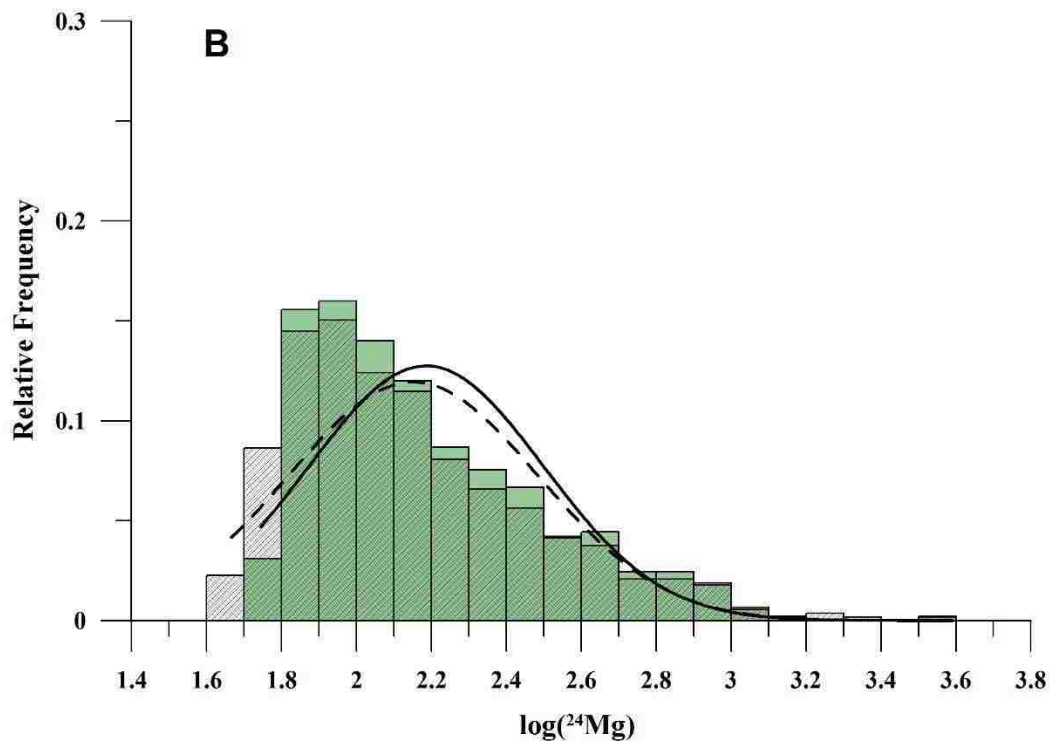
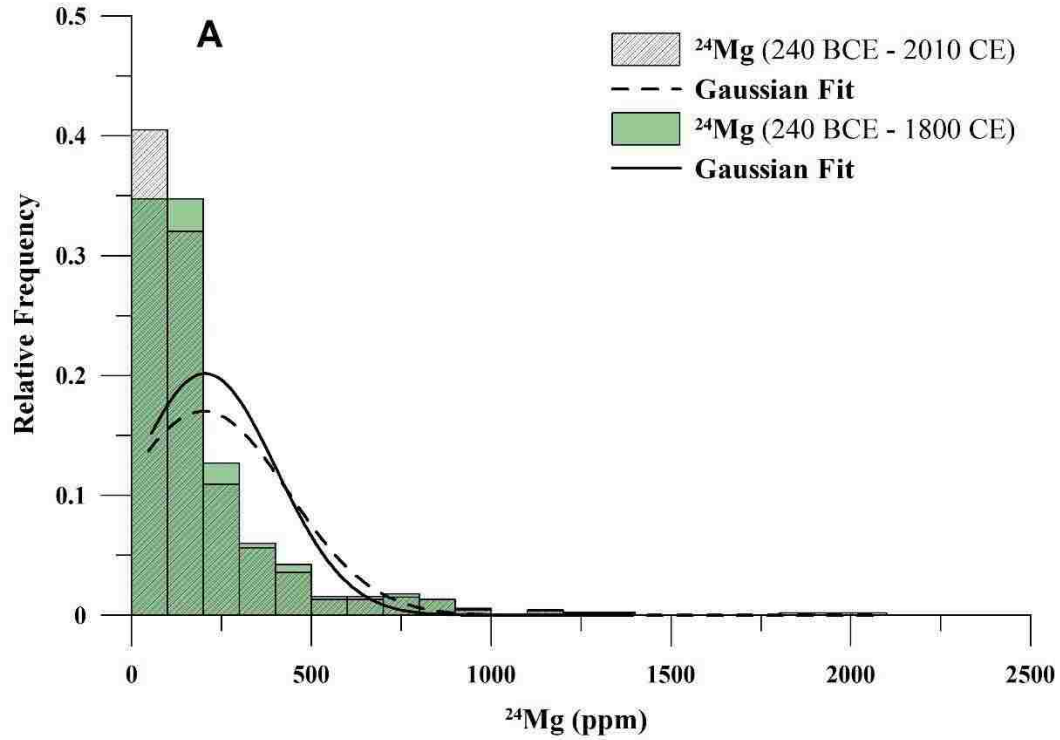


Figure A4 Histograms showing (A) $[^{24}\text{Mg}]$ and (B) $\log(^{24}\text{Mg})$ of JX-6 between 240 BCE – 2010 CE (slashed bars and dashed line) and between 240 BCE – 1800 CE (green bars and solid line). Data separated to show difference in distribution between time periods with and without anomalous spikes in trace element concentrations (1800 – 2010 CE).

References

- Becerra, J. X., 2005, Timing the origin and expansion of the Mexican tropical dry forest: *Proceedings of the National Academy of Sciences of the United States of America*, v. 102, no. 31, p. 10919-10923.
- Borsato, A., Frisia, S., Fairchild, I. J., Somogyi, A., and Susini, J., 2007, Trace element distribution in annual stalagmite laminae mapped by micrometer-resolution X-ray fluorescence: Implications for incorporation of environmentally significant species: *Geochimica et Cosmochimica Acta*, v. 71, no. 6, p. 1494-1512.
- Cerling, T. E., and Quade, J., 1993, Stable carbon and oxygen isotopes in soil carbonates: Climate change in continental isotopic records, p. 217-231.
- Cruz, F. W., Burns, S. J., Jercinovic, M., Karmann, I., Sharp, W. D., and Vuille, M., 2007, Evidence of rainfall variations in Southern Brazil from trace element ratios (Mg/Ca and Sr/Ca) in a Late Pleistocene stalagmite: *Geochimica et Cosmochimica Acta*, v. 71, no. 9, p. 2250-2263.
- Cruz, F. W., Burns, S. J., Karmann, I., Sharp, W. D., Vuille, M., Cardoso, A. O., Ferrari, J. A., Dias, P. L. S., and Viana, O., 2005, Insolation-driven changes in atmospheric circulation over the past 116,000 years in subtropical Brazil: *Nature*, v. 434, no. 7029, p. 63-66.
- Cruz, F. W., Burns, S. J., Karmann, I., Sharp, W. D., Vuille, M., and Ferrari, J. A., 2006, A stalagmite record of changes in atmospheric circulation and soil processes in the Brazilian subtropics during the Late Pleistocene: *Quaternary Science Reviews*, v. 25, no. 21, p. 2749-2761.
- Fairchild, I. J., Borsato, A., Tooth, A. F., Frisia, S., Hawkesworth, C. J., Huang, Y., McDermott, F., and Spiro, B., 2000, Controls on trace element Sr-Mg compositions of carbonate cave waters: implications for speleothem climatic records: *Chemical Geology*, v. 166, p. 255-269.
- Fairchild, I. J., Smith, C. L., Baker, A., Fuller, L., Spötl, C., Matthey, D., McDermott, F., and E.I.M.F., 2006, Modification and preservation of environmental signals in speleothems: *Earth-Science Reviews*, v. 75, no. 1-4, p. 105-153.
- Finch, R. J., and Murakami, T., 1999, Systematics and paragenesis of uranium minerals. In: Burns, P. C., Finch, R. N., (Eds.), *Uranium: Mineralogy, Geochemistry and the Environment*. *Reviews in Mineralogy*, p. 91-180.
- Genty, D., Baker, A., Massault, M., Proctor, C., Gilmour, M., Pons-Branchu, E., and Hamelin, B., 2001, Dead carbon in stalagmites: carbonate bedrock paleodissolution vs. ageing of soil organic matter. Implications for ^{13}C variations in speleothems: *Geochimica et Cosmochimica Acta*, v. 65, no. 20, p. 3443-3457.
- Hellstrom, J., and McCulloch, M., 2000, Multi-proxy constraints on the climatic significance of trace element records from a New Zealand speleothem: *Earth and Planetary Science Letters*, v. 179, no. 2, p. 287-297.

- Hellstrom, J., McCulloch, M., and Stone, J., 1998, A detailed 31,000-year record of climate and vegetation change, from the isotope geochemistry of two New Zealand speleothems: *Quaternary Research*, v. 50, no. 2, p. 167-178.
- Hodell, D. A., Brenner, M., and Curtis, J. H., 2007, Climate and cultural history of the northeastern Yucatan Peninsula, Quintana Roo, Mexico: *Climatic Change*, v. 83, no. 1-2, p. 215-240.
- Huang, Y., and Fairchild, I. J., 2001, Partitioning of Sr^{2+} and Mg^{2+} into calcite under karst-analogue experimental conditions: *Geochimica et Cosmochimica Acta*, v. 65, no. 1, p. 47-62.
- Jauregui, E., 1990, Influence of a large urban park on temperature and convective precipitation in a tropical city: *Energy and Building*, v. 15, p. 457-463.
- Johnson, K., Hu, C., Belshaw, N., and Henderson, G., 2006, Seasonal trace-element and stable-isotope variations in a Chinese speleothem: The potential for high-resolution paleomonsoon reconstruction: *Earth and Planetary Science Letters*, v. 244, no. 1-2, p. 394-407.
- Lachniet, M. S., 2009, Climatic and environmental controls on speleothem oxygen-isotope values: *Quaternary Science Reviews*, v. 28, no. 5-6, p. 412-432.
- Lachniet, M. S., Bernal, J. P., Asmerom, Y., Polyak, V., and Piperno, D., 2012a, A 2400 yr Mesoamerican rainfall reconstruction links climate and cultural change: *Geology*, v. 40, no. 3, p. 259-262.
- Lachniet, M. S., Bernal, J. P., Asmerom, Y., and Polyak, V., 2012b, Uranium loss and aragonite–calcite age discordance in a calcitized aragonite stalagmite: *Quaternary Geochronology*, v. 14, p. 26-37.
- Langmuir, D., 1978, Uranium solution-mineral equilibria at low temperatures with applications to sedimentary ore deposits: *Geochimica et Cosmochimica Acta*, v. 42, no. 6, p. 547-569.
- Linge, H., Lauritzen, S.-E., Lundberg, J., and Berstad, I., 2001, Stable isotope stratigraphy of Holocene speleothems: examples from a cave system in Rana, northern Norway: *Palaeogeography, Palaeoclimatology, Palaeoecology*, v. 167, no. 3, p. 209-224.
- McDermott, F., 2004, Palaeo-climate reconstruction from stable isotope variations in speleothems: a review: *Quaternary Science Reviews*, v. 23, no. 7-8, p. 901-918.
- Meece, D., and Benninger, L., 1993, The coprecipitation of Pu and other radionuclides with CaCO_3 : *Geochimica et Cosmochimica Acta*, v. 57, no. 7, p. 1447-1458.
- Treble, P., Shelley, J.M.G., and Chappell, J., 2003, Comparison of high resolution sub-annual records of trace elements in a modern (1911-1992) speleothem with instrumental climate data from southwest Australia: *Earth and Planetary Science Letters*, v. 216, p. 141-153.
- Reeder, R. J., Nugent, M., Lamble, G. M., Tait, C. D., and Morris, D. E., 2000, Uranyl incorporation into calcite and aragonite: XAFS and luminescence studies: *Environmental science & technology*, v. 34, no. 4, p. 638-644.

- Roberts, M. S., Smart, P. L., and Baker, A., 1998, Annual trace element variations in a Holocene speleothem: *Earth and Planetary Science Letters*, v. 154, no. 1, p. 237-246.
- Romanek, C. S., Grossman, E. L., and Morse, J. W., 1992, Carbon isotopic fractionation in synthetic aragonite and calcite: effects of temperature and precipitation rate: *Geochimica et Cosmochimica Acta*, v. 56, no. 1, p. 419-430.
- Rosales, L., 2013, New cave survey at Grutas de Juxtlahuaca, Mexico: *Association for Mexican Cave Studies Activities Newsletter*, no. 36, p. 63-65.
- Sturchio, N., Antonio, M., Soderholm, L., Sutton, S., and Brannon, J., 1998, Tetravalent uranium in calcite: *Science*, v. 281, no. 5379, p. 971-973.
- Zhou, P., and Gu, B., 2005, Extraction of oxidized and reduced forms of uranium from contaminated soils: effects of carbonate concentration and pH: *Environmental Science and Technology*, v. 39, no. 12, p. 4435-4440.

Curriculum Vitae

CHAD M. CROTTY

Graduate Assistant

University of Nevada, Las Vegas

4505 S. Maryland Pkwy Las Vegas, NV 89154 USA

Phone: (763) 439-8950, E-mail: crotty@unlv.nevada.edu

Education

M.S., Geology, University of Nevada, Las Vegas, Expected: May 2015.

B.S., Geosciences, North Dakota State University, 2011.

Employment History

January 2013–Present: *Graduate Assistant*, University of Nevada, Las Vegas.

Instructed students in two separate laboratory settings on the basics of introductory geology, focusing on rock and mineral identification, and on the principles of geomorphology, focusing on surficial processes and the recognition of landforms using topographic maps and aerial photographs.

November 2011–November 2012: *Research Specialist*, Energy and Environmental Research Center, University of North Dakota. Responsibilities included supporting geology-based geographic information system data development, writing geologic reports, mapping subsurface geology, creating cross sections, maintaining dynamic databases, spatial analysis, and cartographic output.

April 2011–November 2011: *Researcher*, Energy and Environmental Research Center, University of North Dakota. Responsibilities included assisting in the data management of a PETRA Well Database, creating maps using the ESRI Arc 10 product family, and researching and writing reports on geologic subsurface systems.

May 2010–August 2010: *Geology Intern*, Murex Petroleum Corporation, Houston, Texas. Responsibilities included mapping formation tops on the program PETRA using well logs, searching for possible oil traps within specific formations, and calculating the volumetric percentage of fluid within these traps.

January 2010–May 2010: *Teaching Assistant*, North Dakota State University, Fargo, North Dakota. Assisted students in understanding fundamental concepts of geology in a laboratory setting and graded reports with an emphasis on sedimentology and stratigraphy.

Field Experience

November 2014: Great Basin National Park, Nevada. Assisted in the mapping of a section of Lehman Cave using the compass and tape method in cooperation with the Southern Nevada Grotto.

October 2010–December 2010: Transantarctic Mountains, Antarctica. Assisted in the mapping of glacial deposits and the collection of Neogene fossiliferous deposits in multiple remote field camps in the Transantarctic Mountains.

Summer 2008 & Fall 2010: Eastern North Dakota. Assisted in the collection of samples from Glacial Lake Agassiz strandlines to be processed in the Optical Dating and Dosimetry Laboratory, Department of Geosciences, North Dakota State University.

Publications and Presentations

Peck, W.D., Bachu, S., Knudsen, D.J., Hauck, T., **Crotty, C.M.**, Gorecki, C.D., Sorensen, J.A., Talman, S., Peterson, J., and Melnik, A., 2012, CO₂ storage resource potential of the Cambro–Ordovician saline system in the western interior of North America [abs.]: 11th International Conference on Greenhouse Gas Control Technologies (GHGT-11), Kyoto, Japan, November 18–22, 2012.

Peck, W.D., **Crotty, C.M.**, Knudsen, D.J., Sorensen, J.A., Gorecki, C.D., and Steadman, E.N., 2012, Geological characterization of the Basal Cambrian system in the Williston Basin: Plains CO₂ Reduction (PCOR) Partnership Phase III Task 16 Deliverable D91 for U.S. Department of Energy National Energy Technology Laboratory Cooperative Agreement No. DE-FC26-05NT42592, EERC Publication 2012-EERC-04-19, Grand Forks, North Dakota, Energy & Environmental Research Center, February.

Peck, W.D., Knudsen, D.J., **Crotty, C.M.**, Sorensen, J.A., Gorecki, C.D., Bachu, S., Hauck, T., and Peterson, J., 2012, CO₂ storage resource potential of the Cambro-Ordovician saline system in the western interior of North America [abs.]: 11th Annual Conference on Carbon Capture Utilization & Sequestration, Pittsburgh, Pennsylvania, April 30 – May 3, 2012.